Click here to view PowerPoint presentation; Press Esc to exit

What Can We Learn About the Ionosphere Using the EISCAT Heating Facility?

Michael T. Rietveld
EISCAT Scientific Association
Ramfjordmoen
N-9027 Ramfjordbotn

mike.rietveld@eiscat.uit.no

ABSTRACT

Apart from being used for plasma physics, the HF facility near Tromsø, Norway, can be used to perturb the ionosphere at various heights in different ways, thereby giving information about the ionosphere. The co-located incoherent scatter radars are probably the most powerful instrument for probing the ionosphere, but HF techniques can complement the radars and even have some advantages. The principal perturbation method is to increase the electron temperature in a controlled way, some examples of which are presented here.

Artificial electron heating in the E and F regions is useful for testing aeronomical models. More recently it has been discovered that electron heating can dramatically affect polar mesospheric echoes observed by VHF and UHF radars. Particularly the overshoot effect promises to be a powerful diagnostic of the physics and chemistry related to the formation of these layers, which are thought to involve dust, ice particles and aerosols.

Radio induced optical emissions provide a way of measuring the lifetimes of excited species at different heights in the ionosphere, thereby providing a way of measuring the neutral density which is one of the most important parameters determining the lifetime.

The technique of creating artificial periodic irregularities set up in the standing wave pattern of the up-going and ionospherically reflected HF wave provides valuable information all heights below reflection. One particular feature of this method is that it can detect the presence of layers around 50 km and measure vertical winds, and electron densities and temperatures at various heights.

1.0 INTRODUCTION

Dedicated powerful HF radio wave transmitting facilities have been in use since the 1970s to do both plasma physics and geophysical research. At present there are five operating facilities: HIPAS [1] and HAARP [2] in Alaska, Heating in northern Norway [3], SPEAR on the island if Spitsbergen [4] and SURA in Russia [5]. Another important facility in Puerto Rico [6] was damaged by a hurricane in 1996 but there are plans to build a replacement. Although incoherent radar, which is often co-located with such a powerful HF facility, is recognised as being the most powerful technique for measuring ionospheric and to some extent atmospheric properties, its capabilities can often be extended by using ionospheric perturbation techniques. HF-modification facilities, which themselves are much less expensive than incoherent scatter radars, can also be used together with even less expensive HF or VHF coherent scatter radars or other diagnostics to probe the ionosphere and even magnetosphere as will be shown below.

By perturbing the ionosphere in a controlled way and measuring the effect with some other instrument, it is possible to learn something about the properties of the ionospheric plasma or the neutral atmosphere.

Rietveld, M.T. (2006) What Can We Learn About the Ionosphere Using the EISCAT Heating Facility? In *Characterising the Ionosphere* (pp. 25-1 – 25-10). Meeting Proceedings RTO-MP-IST-056, Paper 25. Neuilly-sur-Seine, France: RTO. Available from: http://www.rto.nato.int/abstracts.asp.

Report Documentation Page

Form Approved
OMB No. 0704-0188

1. REPORT DATE	2. REPORT TYPE	3. DATES COVERED
01 JUN 2006	**N/A**	**-**

4. TITLE AND SUBTITLE	5a. CONTRACT NUMBER
What Can We Learn About the Ionosphere Using the EISCAT Heating Facility?	5b. GRANT NUMBER
	5c. PROGRAM ELEMENT NUMBER
6. AUTHOR(S)	5d. PROJECT NUMBER
	5e. TASK NUMBER
	5f. WORK UNIT NUMBER
7. PERFORMING ORGANIZATION NAME(S) AND ADDRESS(ES) **EISCAT Scientific Association Ramfjordmoen N-9027 Ramfjordbotn**	8. PERFORMING ORGANIZATION REPORT NUMBER
9. SPONSORING/MONITORING AGENCY NAME(S) AND ADDRESS(ES)	10. SPONSOR/MONITOR'S ACRONYM(S)
	11. SPONSOR/MONITOR'S REPORT NUMBER(S)

12. DISTRIBUTION/AVAILABILITY STATEMENT
Approved for public release, distribution unlimited

13. SUPPLEMENTARY NOTES
See also ADM002065., The original document contains color images.

14. ABSTRACT

15. SUBJECT TERMS

16. SECURITY CLASSIFICATION OF:			17. LIMITATION OF ABSTRACT	18. NUMBER OF PAGES	19a. NAME OF RESPONSIBLE PERSON
a. REPORT	b. ABSTRACT	c. THIS PAGE			
unclassified	**unclassified**	**unclassified**	**UU**	**40**	

Standard Form 298 (Rev. 8-98)
Prescribed by ANSI Std Z39-18

There are several ways of causing a perturbation with a powerful HF radio wave. The absorption of the wave causes electron heating, which is perhaps the most direct way, and will be discussed in section 2. Another way is to directly excite plasma waves which are localised in their source height by resonance conditions. If the plasma waves are Langmuir or ion acoustic waves they can be measured by incoherent scatter radars and allow accurate calibration of electron densities and temperatures. The associated plasma turbulence can also energize electrons such that they cause the atmospheric molecules to emit light. These plasma wave effects are discussed in Section 3. Modulated electron heating can be used to create low frequency ionospheric currents which are in turn useful for studying the properties of the ionosphere or the coupled ionosphere-magnetosphere system, as discussed in Section 4. Heating effects can also be used to track the ionospheric electric field of naturally-occurring ULF waves, as demonstrated in the same section. Finally, in Section 5 a technique is described where periodic irregularities set up in the standing wave of the reflected HF pump are used as a tracer for ionospheric parameters from the F region down to extremely low heights like 50 km.

2.0 ELECTRON HEATING

A powerful HF is absorbed in the D region through collisions or simple Ohmic heating. Models predict temperature enhancements up to many hundreds or even thousands of degrees, but direct measurements of this by means of incoherent scatter radar has proved impossible to verify so far. Nevertheless the effects of electron heating at heights between about 60 and 90 km are evident. Examples are the modulation of the electron collision frequency and hence conductivities and electric currents by amplitude modulated heating at frequencies from sub-Herz to kHz, as described in Section 4. Heating effects in the E region also exist but have also been difficult to measure [7]. Heating effects in the F region can be strong through anomalous absorption of the HF wave caused by electrostatic instabilities, and have been well documented [8, 9]. We now discuss the diagnostic applications of D region and F region heating.

2.1 The effect of electron heating on the mesosphere

The mesosphere is that region of the atmosphere between about 50 and 85 km where the temperature decreases with altitude and reaches a minimum at around 85 km. It is difficult to access this region except through sounding rockets or radars. Radar echoes require sufficient electron density which is provided through ionising sunlight, precipitating energetic electrons through magnetospheric acceleration processes such as that associated with the aurora, or protons during energetic solar eruptions. When there are sufficient electrons, they can be structured on various spatial scales by turbulence, or by attachment to aerosols such as ice and dust particles, thereby acting as passive tracers of the neutral atmosphere and its inhomogeneities. VHF and occasionally UHF radar echoes which are seen commonly in the polar mesosphere at heights from 80 to 90 km, known as Polar Mesospheric Summer Echoes (PMSE) [10, 11] are still not understood. Weaker and rarer echoes are also seen from lower heights around 70 km, sometimes termed Polar Mesosphere Winter Echoes (PMWE) [12].

Chilson et al. [13] found that the strength of PMSE echoes could be weakened by up to 10 dB by transmitting a powerful HF wave of several hundred MW effective radiated power (ERP). The response time was practically instantaneous [14] suggesting that electron heating, which has a time constant of tens to hundreds of microseconds in these heights [15], caused the weaker echoes. The weakening of the echoes is caused by the increased diffusivity of the hotter electrons smearing out the small (meter) scale structuring of the electrons [16]. More recently O. Havnes predicted that that by using a lower duty cycle modulation, it should also be possible to enhance the strength of the echoes [17]. The effect which was immediately found [18] and which is shown in Fig.1, promises to be an important diagnostic of the mesosphere and D region. This is because, as Fig. 2 shows, the overshoot characteristic curve depends on the aerosol size used in the model. Figure 2 shows two cases computed for a plasma density $n_0 = 4 \times 10^9$ m^{-3} and an increase in the electron temperature from 150 K without heating, to 390 K with heating. The

level of suppression (0 to 1 in Fig.2) depends on the temperature enhancement. Two different dust sizes were used in the figure. The dust density is $n_d = 10^9$ m^{-3} for the case with particles of radius r = 10 nm (solid line) and $n_d = 4 \times 10^7$ m^{-3} for the 50 nm large particles (dashed line).

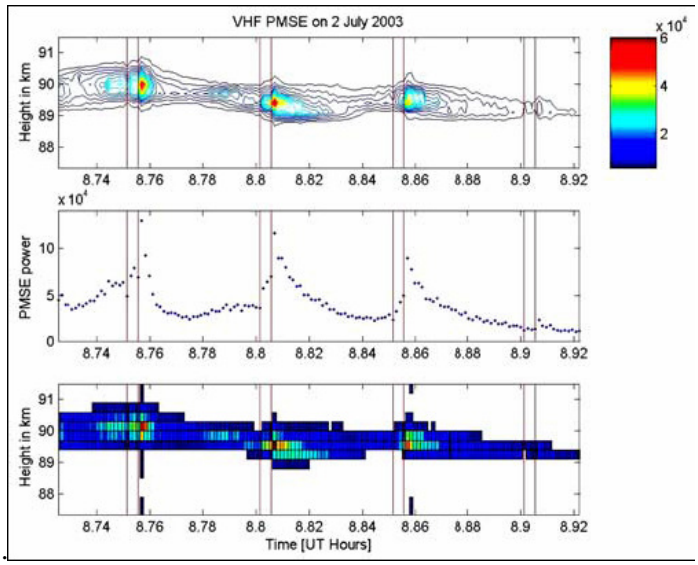

Figure 1: PMSE echo strength showing an overshoot immediately after switch the 3s long heater pulse off. HF on is shown by the vertical lines. The bottom panel shows the raw data, corrected for radar transmitter power, while the upper panel shows the same data but now smoothed. The relative intensity scale is the same for both panels, and the background noise on this linear scale is at approximately 2500. The middle panel shows the sum of the three highest intensities at each time sample and is a measure of the total PMSE intensity as a function of time. Taken from [18].

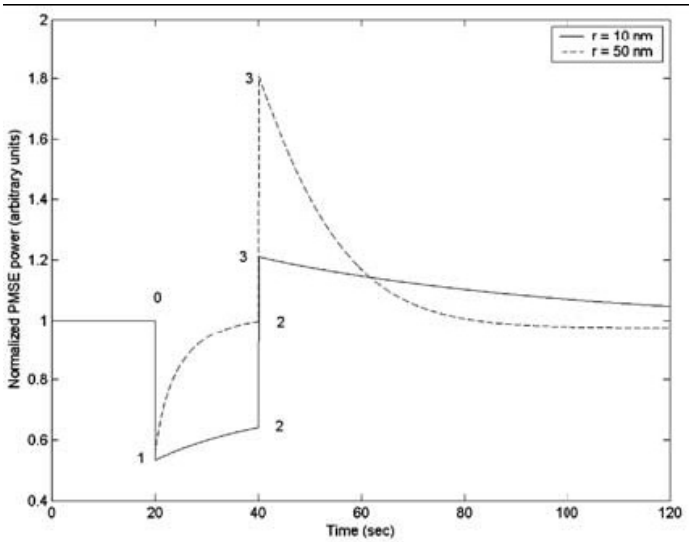

Figure 2: Model calculations showing how the shape of the overshoot phenomenon depends on particle size. HF is on from 20 to 40 s and the amplitude from 0 to 1 depends on the electron heating. Taken from [18].

2.2 Heating effects in the F region

Measurements of HF-induced electron heating in the F-region were first analysed in detail by Mantas et al. [8]. Such measurements provide useful tests of models of the thermal balance of the electron and ion gas in the ionosphere. If one neglects particle concentration changes then only the coupled time-dependent heat equations for the electron and ion gas need to be solved. A large error in the assumed electron energy loss rates through the various collision mechanisms can be detected by comparing the observed with the calculated decay rate of the enhanced electron temperature profile after turning the HF wave off [8].

2.2.1 Artificial optical emissions

Artificial optical emissions from the F region (and E region) can be induced by high power radio waves. The easiest emission to be observed is the red line at 630 nm from O(^{1}D) which has an excitation threshold energy of 1.97 eV , followed by the green line at 577.7 nm from O(^{1}S) with an effective energy threshold of 4.19 eV but lines have also been observed at 844.6 nm, from O(3p^{3}P) with threshold of 10.99 eV and at 427.8 nm with threshold 18 eV from N_2^+ [19]. There seem to be two mechanisms involved. The first is the reasonably well understood thermal heating of the electrons causing the Maxwellian tail to be enhanced [8]. With electron heating of 2000-4000K this mechanism can explain the 630 nm red-line emission of atomic oxygen which has the lowest excitation energy. The other mechanism, which is not well understood, is the acceleration of thermal electrons to supra-thermal energies of up to a few tens of eV by a process involving plasma waves. This second mechanism seems necessary to explain the green line atomic oxygen emission and other emissions with higher energy thresholds.

Whatever the mechanism, it is possible to create a cloud of excited atomic oxygen atoms which can be used to determine thermospheric properties as described by [20]. For example, steady state heating causes the cloud of optical emission to move with the plasma velocity ($\mathbf{E} \times \mathbf{B}$ drift) and show the irregularity structure of the plasma. When the radio wave is turned off, the cloud expands by neutral diffusion drifts and drifts with the neutral wind velocity as the intensity decays on a timescale of tens of seconds. The decay rate is determined by the collisional quenching rate and both diffusion quenching rates are directly related to the atomic and molecular concentrations in the thermosphere. Whereas the neutral wind probably does not vary much with height, the neutral density decreases with height causing the lifetime of the excited O state and the diffusion rate to decrease with height. Thus by measuring the decay of artificial red line emissions at different heights one could obtain a height profile of the neutral density. Some initial measurements which could be used in an attempt to do this is shown in Figure 3, taken from [21], where the optical emission height increased as the ionosphere decayed after sunset. In such experiments it is necessary to determine the height of the optical emissions by triangulation using several cameras. The source height of the electron heating or electron acceleration, which is the upper-hybrid resonance height which is close to but below the HF reflection height, can usually be determined from ionosonde or radar measurements.

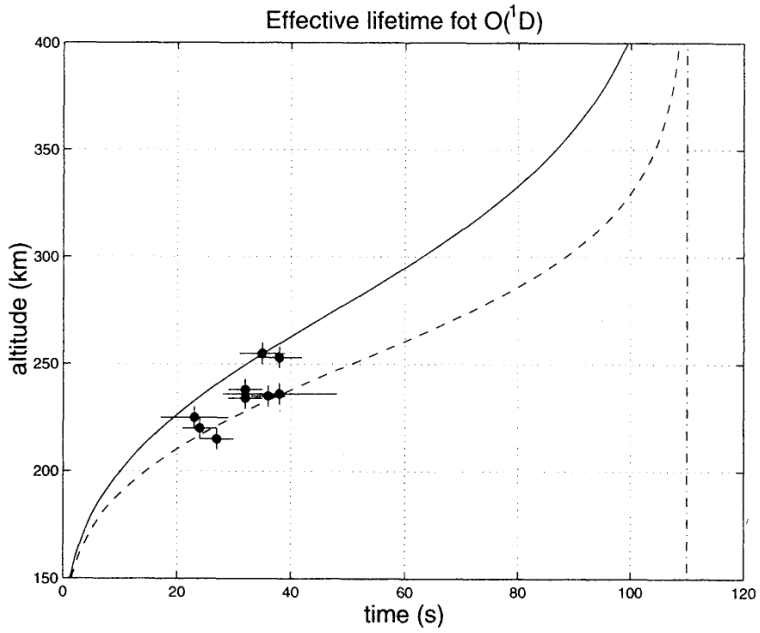

Figure 3: Altitude variation of the decay time constants of O(^{1}D) from [24]. The dot-dashed line shows the radiative lifetime of O(^{1}D), the dashed curve including quenching by O_2, N_2 and ambient electrons, the solid curve including quenching by atomic oxygen. The markers show estimates of the time constant from the experiment described in [21].

3.0 PLASMA WAVE EXCITATION

The electric field of the powerful HF wave becomes even stronger near the reflection height as a result of the decreasing refractive index. It can decay into ion acoustic and Langmuir waves both of which may be detected by incoherent scatter radars and thereby provide a strong signal, in a usually very narrow range extent which is ideal for calibrating electron density measurement of such radars. Often it is even possible to obtain such enhanced ion and plasma lines on the topside ionosphere, through tunnelling of the HF wave in the Z-mode [Isham ?].

4.0 ULF, ELF, VLF WAVE EXCITATION AND DETECTION

4.1 Excitation of ELF/VLF waves

The production of ELF/VLF waves (from hundreds of Hz to many kHz) by modulated heating and thereby conductivity modulation in the lower layers of the ionosphere allows a number of diagnostic techniques. An advantage of this source of low frequency waves is its wide instantaneous bandwidth in spite of the low efficiency [22]. One approach is to use the radiated ELF/VLF waves propagating in the Earth-ionosphere waveguide to test models of propagation and models of the lower ionosphere, as done by Barr et al. for example [23].

The nonlinear relationship between electron temperature enhancement and HF energy input depends on the loss mechanism of the heated electrons. For small electron temperature enhancements, rotational excitation of N_2 and O_2 is the most efficient energy loss mechanism. Its temperature dependence is known to be $(T_e - T_n)/T_e^{1/2}$ where T_e and T_n are the electron and neutral temperatures respectively Since the collision frequency v_e is approximately proportional to T_e, there exists an altitude above which the HF

absorption coefficient increases with T_e more strongly than $T_e^{1/2}$ It is obvious that in this case there is a critical energy input above which the loss cannot compensate the gain. Correspondingly, a runaway solution for T_e arises, which is eventually limited by other energy loss mechanisms, mainly vibrational excitation of N_2 and O_2. This relationship could be measured by seeing how the amplitude of waves at a fixed ELF/VLF modulation frequency having a fixed modulation depth varies as the average HF level is increased, as outlined in [24]. Although there have been many ELF/VLF modulation experiments performed over the years, this particular one has not been done, but it could provide the shape of the T_e vs. HF-power curve which one should be able to relate to the model containing the height profile of $[O_2]$,$[N_2]$ and T_n.

4.2 Excitation of ULF waves

The production of ULF waves below about 10 Hz is particularly interesting because there are so few alternative artificial sources. These waves, as they propagate into the magnetosphere as Alfvén waves can be very efficiently guided along the magnetic field to satellites and thereby provide a tracer of the field line [25, 26] They may also be used to actively study the ionospheric Alfvén resonator. [27, 28, 29].

4.3 Detection of ULF waves using heating

There are at least two ways of detecting the ionospheric signature of naturally occurring ULF pulsations. The first way is by the fact that the electric field of the natural ULF wave modulates the current system in the lower ionosphere thereby imparting its frequency on any ELF or VLF waves that may be produced by artificial modulation of those currents. Signatures of natural Pc 4 and Pc 1 ULF waves were thus found on ELF/VLF waves produced by the HF facility and recorded on the ground nearby [30, 31]. These ULF waves were also seen by ground-based magnetometers.

Another, more interesting technique can be used to detect the ionospheric signature in the F region of pulsations that have such a localised spatial scale that they are not normally observable by ground based magnetometers because of the shielding effect of the ionosphere. It involves generating decameter scale irregularities near the upper-hybrid resonance height using o-mode heating, and then detecting the movement of the irregularities with coherent radars like SUPER DARN as shown in [32]. The horizontal electric fields of the pulsation cause an $\mathbf{E} \times \mathbf{B}$ force on the plasma containing the artificial irregularities resulting in a Doppler shift of coherently scattered radar signals. The artificial irregularities have a very narrow intrinsic backscatter spectrum [33], allowing high precision measurements of the drifts.

5.0 PROBING OF ARTIFICIAL PERIODIC IRREGULARITIES

A particularly powerful method of using heating facilities to probe the ionosphere from the reflection height of the HF wave down to 50 km or so is the artificial periodic irregularity (API) technique developed by a Russian group using the SURA HF facility [34]. The technique relies on the standing wave pattern created by the by the HF wave and its reflection causing a horizontally stratified periodic perturbation to the refractive index which is then probed by pulsed HF radio waves matching the Bragg scattering criterion. This probing can be performed with the same frequency and polarisation as the pump wave so that the Bragg condition is met at all heights. In this case the probing can only be done to watch the irregularity pattern decay immediately after the pump switches off. Alternatively, the probing can be done with another frequency and polarization such that the Bragg condition is met over a narrow range of heights, but while the pump wave is on. The first mode is appropriate for D region heights where the time constant for irregularities to decay is generally long enough. An example is shown in Fig. 4 where irregularities are formed in two height regions, 80-100 km and 50-60 km and decay with different time constants which are determined by the ion chemistry [35].

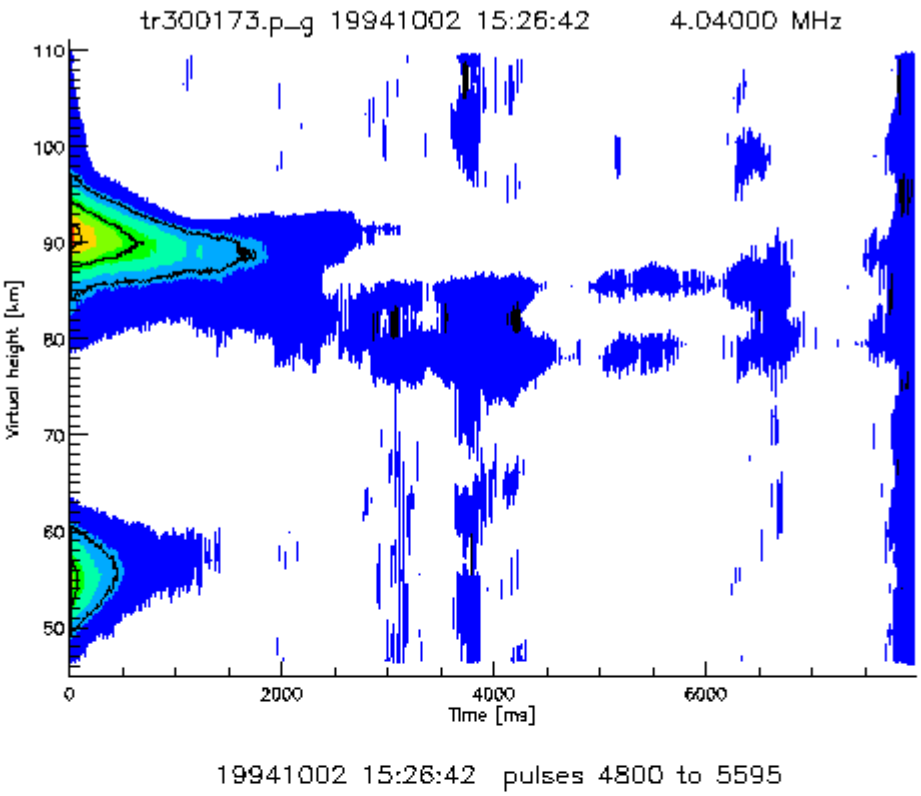

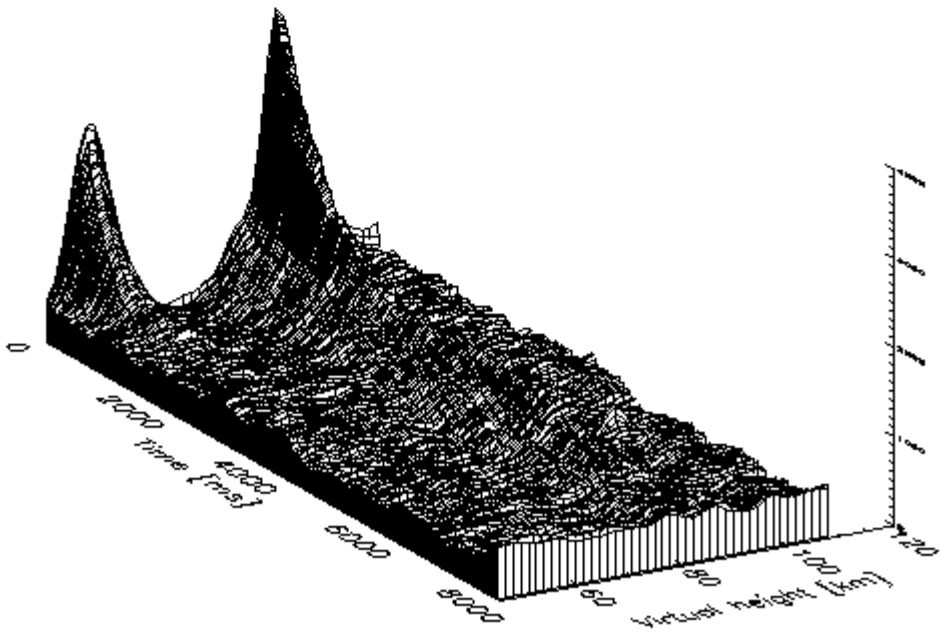

Figure 4: Very low altitude echoes from decaying irregularities after turning off the standing

wave pattern caused by the powerful HF wave and its ionospheric reflection.

6.0 SUMMARY

I have presented some examples of HF-heating of the ionosphere can be used to learn about the ionosphere and even magnetosphere. Most of the techniques have been tried to some extent, but there is a large potential to exploit them in a more systematic way.

7.0 REFERENCES

[1] Wong, A. Y., Carroll, J., Dickman, R. et. al. (1990). High-power radiating facility at the HIPAS observatory, Radio Science, 25, 1269-1282.

[2] Pedersen, T. R., & Carlson, H. C. (2001). First observations of HF heater-produced airglow at the High Frequency Active Auroral Research Program facility: Thermal excitation and spatial structuring Radio Sci., 36, 5, 1013-1026.

[3] Rietveld, M. T., Kohl, H. Kopka, H., & Stubbe, P. (1993). Introduction to ionospheric heating experiments at Tromsø Part 1: Experimental overview, J. Atmos. Terr. Phys., 55, 577-599.

[4] Robinson, T. R., Yeoman, T. K., Dhillon, R. S., Lester, M., Thomas, E. C., Thornhill, J. D., Wright, D. M., van Eyken, A. P., & McCrea, I. (2006). First observations of SPEAR induced artificial backscatter from CUTLASS and the EISCAT Svalbard radar, Annales Geophysicae, 24, 291-309.

[5] Frolov V. L., Sergeev, E. N., Komrakov, G. P., Stubbe, P., Thidé, B., Waldenvik, M., Veszelei, E., & Leyser, T. B. (2004). Ponderomotive narrow continuum (NC p) component in stimulated electromagnetic emission spectra, J. Geophys. Res., 109, A07304, doi:10.1029/2001JA005063.

[6] Fejer, J. A., Sulzer, M. P., & Djuth, F. T. (1991). Height dependence of the observed spectrum of radar backscatter from HF-Induced ionospheric langmuir turbulence, J. Geophys. Res., 96(A9), 15985-16008.

[7] Robinson, T. R., Bond, G., Eglitis, P., Honary, F., & Rietveld, M. T. (1998). RF heating of a strong auroral electrojet, Adv. Space Res., 21, 5, 689-692.

[8] Mantas, G. P., Carlson Jr., H. C., & LaHoz, C. H. (1981). Thermal response of the F region ionosphere in artificial modification experiments by HF radio waves, J. Geophys. Res., 86, 561-574.

[9] Rietveld, M. T., Kosch, M. J., Blagoveshchenskaya, N. F., Kornienko, V. A., Leyser, T. B., Yeoman, T. K. (2003). Ionospheric electron heating, optical emissions and striations induced by powerful HF radio waves at high latitudes: aspect angle dependence, J. Geophys. Res., 108, A4, (SIA 2-1 to SIA 2-16), 1141, doi:10.1029/2002JA009543.

[10] Röttger, J., LaHoz, C., Kelley, M. C., Hoppe, U.-P., & Hall, C., (1988). The structure and dynamics of polar mesosphere summer echoes observed with the EISCAT 224-MHz radar, Geophys. Res. Lett., 15, 1353-1356.

[11] Cho, J, Y. N., & Kelley, M. C. (1993). Polar mesosphere summer radar echoes: Observations and

current theories, Rev. Geophys., 31, 3, .243-265.

[12] Kirkwood, S., Barabash, V., Belova, E., Nilsson, H., Rao, T. N., Stebel, K., Osepian, A., & Chilson, P. B. (2002). Polar mesosphere winter echoes during solar proton events, Advances in Polar Upper Atmosphere Research, 16, 111-125.

[13] Chilson, P. B., Belova, E., Rietveld, M. T., Kirkwood, S., & Hoppe, U.-P. (2000). First artificially induced modulation of PMSE using the EISCAT heating facility, Geophys. Res. Lett., 27, 23, 3801-3804.

[14] Belova, E., Chilson, P. B., Kirkwood, S., & Rietveld, M. T. (2003). The response time of PMSE to ionospheric heating, J. Geophys. Res. 108, D8, (PMR 13-1 to PMR 13-6), 8446, doi:10.1029/2002JD002385.

[15] Rietveld, M. T., Kopka, H., & Stubbe, P. (1986). D-region characteristics deduced from pulsed ionospheric heating under auroral electrojet conditions, J. Atmos. Terr. Phys., 48, 4, 311-326.

[16] Rapp, M., & Lübken, F.-J. (2000). Electron temperature control of PMSE, Geophys. Res. Lett., 27, 20, 3285-3288.

[17] Havnes, O. (2004). Polar Mesospheric Summer Echoes (PMSE) overshoot effect due to cycling of artificial electron heating, J. Geophys. Res., 109, A02309, doi:10.1029/2003JA010159.

[18] Havnes, O., La Hoz, C., Naesheim, L. I., & Rietveld, M. T. (2003). First observations of the PMSE overshoot effect and its use for investigating the conditions in the summer mesosphere, Geophys Res. Lett. 30, 23, 2229, doi:10.1029/2003GL018429.

[19] Gustavsson, B., Sergienko, T., Kosch, M. .J, Rietveld, M. T., Brändström, B. U. E., Leyser, T. B., Isham, B., Gallop, P., Aso, T., Ejiri, M., Grydeland, T., Steen, Å., LaHoz, C. Kaila, K., Jussila, J., & Holma, H. (2005). The electron energy distribution during HF pumping, a picture painted with all colors, Ann. Geophysicae, 23, 1747-1754.

[20] Bernhardt, P. A., Wong, M., Huba, J. D., Fejer, B. G.,Wagner, L. S., Goldstein, J. A., Selcher, C. A., Frolov, V. L., and Sergeev, E. N. (2000). Optical remote sensing of the thermosphere with HF pumped artificial airglow, J. Geophys. Res., 105, 10 657-10 671.

[21] Gustavsson, B., Sergienko, T., Rietveld, M. T., Honary, F., Steen, Å., Brändström, B. U. E. Leyser, T. B., Aruliah, A. L. Aso, T., Ejiri, M., & Marple, S. (2001). First tomographic estimate of volume distribution of HF-pump enhanced airglow emission, J. Geophys. Res., 106, A12, 29105-29124.

[22] Barr, R., Rietveld, M. T., Kopka, H., Stubbe, P., & Nielsen, E. (1985). Extra-low-frequency radiation from the polar electrojet antenna, Nature, 317, 6033, 155-157.

[23] Barr, R., Stubbe, P., Rietveld, M. T., & Kopka, H. (1986). ELF and VLF Signals Radiated by the 'Polar Electrojet Antenna': Experimental Results, J. Geophys. Res., 91, A4, 4451-4459.

[24] Stubbe, P., Kopka, H., Rietveld, M. T., & Dowden, R. L. (1982). ELF and VLF wave generation by modulated heating of the current carrying lower ionosphere, J. Atmos. Terr. Phys., 44, 12, 1123-1135.

[25] Robinson, T. R., Strangeway, R., Wright, D. M., Davies, J. A., Horne, R. B., Yeoman, T. K., Stocker, A. J., Lester, M., Rietveld, M. T., Mann, I. R., Carlson, C. W., & McFadden, J. P. (2000).

FAST observations of ULF waves injected into the magnetosphere by means of modulated RF heating of the auroral electrojet. Geophys. Res. Lett. 27, 3165-3168.

[26] Wright, D. M., Davies, J. A., Robinson, T. R., Yeoman, T. K., Lester, M., Cash, S. R., Kolesnikova, E., Strangeway, R., Horne, R. B., Rietveld, M. T., & Carlson, C. W. (2003). The tagging of a narrow flux tube using artificial ULF waves generated by modulated high power radio waves. J. Geophys. Res. 108, 1090, doi:10.1029/2002JA009483.

[27] Cash, S. R., Davies, J. A., Kolesnikova, E., Robinson, T. R., Wright, D. M., Yeoman, T. K., Strangeway, R. J. (2002). Modelling electron acceleration within the IAR during a 3 Hz modulated EISCAT heater experiment and comparison with FAST satellite electron flux data. Ann. Geophys., 20, 1499-1507.

[28] Kolesnikova, E., Robinson, T. R., Davies, J. A., Wright, D. M., Lester, M. (2002). Excitation of Alfvén waves by modulated HF heating of the ionosphere, with application to FAST observations. Ann. Geophys., 20, 57-67.

[29] Bösinger, T., kero, B., Pollari, P., Pashin, A., Belyaev, P., Rietveld, M., Turunen, T., & Kangas, J. (2000). Generation of artificial magnetic pulsations in the Pc1 frequency range by periodic heating of the Earth's ionosphere: indications of Alfvén resonator effects, J. Atmos Solar Terr. Physics., 62, 4, 277-297.

[30] Rietveld, M. T., Kopka, H., Nielsen, E., Stubbe, P., & Dowden, R.L. (1983). Ionospheric electric field pulsations: a comparison between VLF results from an ionospheric heating experiment and STARE. J. Geophys. Res. 88, 2140-2146.

[31] Rietveld, M. T., Kopka, H., & Stubbe, P. (1988). Pc1 ionospheric electric field oscillations. Ann. Geophys. 6, 381-388.

[32] Wright, D. M., & Yeoman, T. K. (1999). High-latitude HF Doppler observations of ULF waves. 2. Waves with small spatial scale sizes. Ann. Geophys. 17, 868-876.

[33] Eglitis, P., Robinson, T. R., Rietveld, M. T., Wright, D. M., & Bond, G. E., (1998). The phase speed of artificial field-aligned irregularities observed by CUTLASS during HF modification of the auroral ionosphere, J. Geophys. Res., 103 , A2, 2253-2259.

[34] Belikovich, V. V., Benediktov, E. A., Tolmacheva, A. V., & Bakhmet'eva, N. V. (2002). Ionospheric research by means of artificial periodic irregularities, English edition (translated by Förster, M. and Rietveld, M. T.), Copernicus GmbH (D-37191 Katlenburg-Lindau, Germany), ISBN 3-936586-03-9, 160 pages, 2002.

[35] Rietveld, M. T., E. Turunen, H. Matveinen, N. P. Goncharov & P. Pollari, P. (1996). Artificial Periodic Irregularities in the Auroral Ionosphere, Ann. Geophysicae 14, 1437-1453.

What Can We Learn About the Ionosphere Using the EISCAT Heating Facility?

Michael T. Rietveld

EISCAT Scientific Association
Ramfjordmoen
N-9027 Ramfjordbotn
mike.rietveld@eiscat.uit.no

IST056 Workshop "Characterising the Ionosphere", Fairbanks, 12-16 June 2006

History

The use of HF-heating to diagnose the ionosphere started with the discovery of the Luxembourg effect by Tellegen in 1933, and its explantion by Bailey and Martyn (1934), namely that powerful LF or HF radio waves heat the electrons in the lower ionosphere and thereby affect the absorption coefficient of other radio waves.

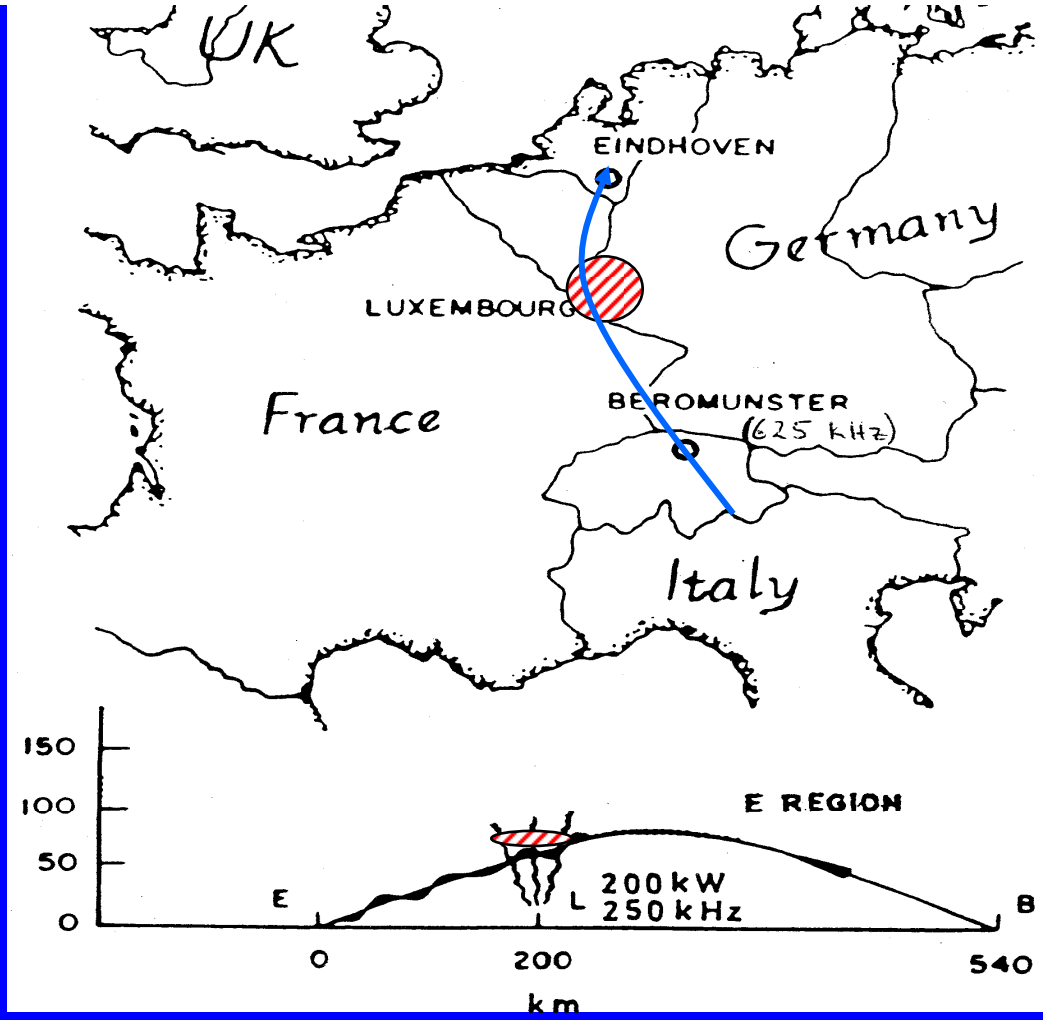

This led to the cross-modulation technique of probing the lower ionosphere, as typified by Fejer (1955).

Results of cross-modulation experiment (Fejer, 1955)

X-mode disturbing wave

O-mode disturbing wave

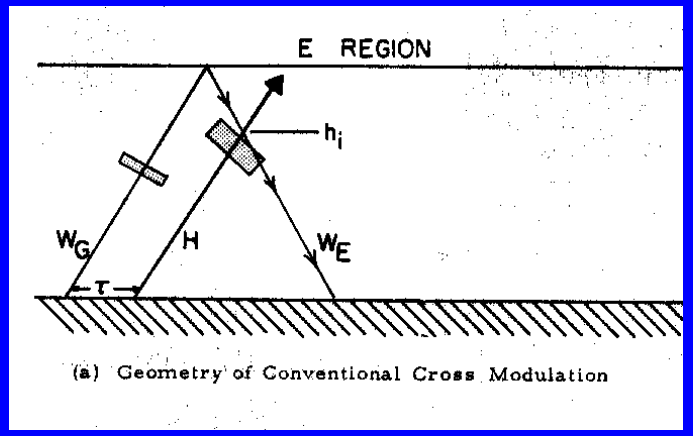

(a) Geometry of Conventional Cross Modulation

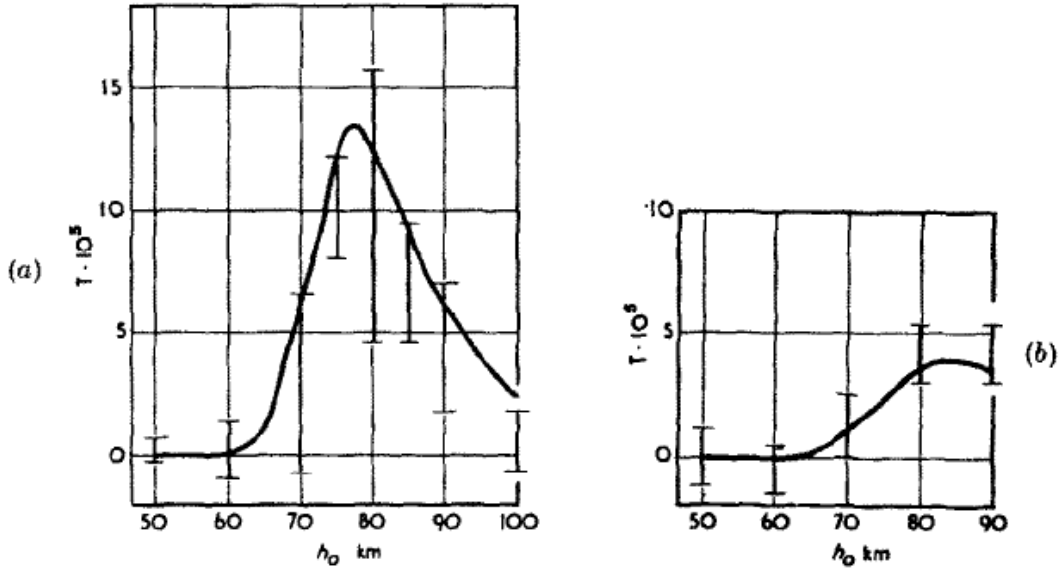

Fig. 3. Mean values and standard deviations of records for different values of h_0. Fig. 3a represents records taken with extraordinary polarization, Fig. 3b records taken with ordinary polarization of the disturbing wave. The lengths of the vertical lines are equal to twice the standard deviation, their midpoints indicate mean values. The solid theoretical curve corresponds to the conditions of Fig. 4.

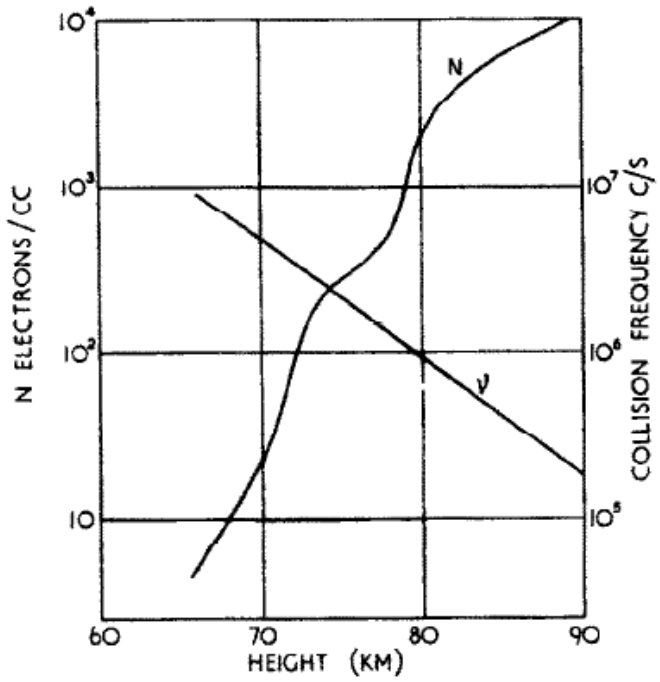

Fig. 4. Collision frequencies and electron densities derived from the experimental data of Fig. 3.

World overview

- 1970: **Platteville**, Colorado
- 1975: **SURA** (Nizhni Novgorod), Russia
- ~1980: **Arecibo** (Puerto Rico), **Tromsø** (Norway), **HIPAS** (Alaska)
- 1995: **HAARP** (Alaska)
- 2003: **SPEAR** (Svalbard)

A comparison

( ) means planned	Plateville Colorado USA	Arecibo Puerto Rico	**HIPAS Alaska USA**	**HAARP Alaska USA**	**Tromsø Norway**	**SURA Russia**	**SPEAR Spitsbergen Norway**
Geographic Coordinates	40.18 N 104.73 E	18.3 N 66.8 W	**65.0 N 147.0 W**	**62.39 N 145.15W**	**69.6 N 19.2 E**	**59.13N 46.1 E**	**78.9 N 78.15 W**
Magnetic Latitude	49.1 N	32 N	**76 N**	**63.09 N**	**67 N**	**50 N**	
Frequency [MHz]	2.8-10	3-12	**2.8-5**	**2.8-8 (2.8-10)**	**4-5.5 5.5-8**	**4.5-9**	**4-6 (2-3)**
Radiated Power [MW]	2	0.8	**1.6**	**0.96 (3.6)**	**1.0**	**0.75**	**0.19**
Antenna Gain [dB]	19	23-26	**18-19**	**14-24 (31)**	**22-25 28-31**	**23-26**	**22 (16)**
Effective Radiated Power [MW]	100	160	**130**	**11-170 (4000)**	**180-340 630-1260**	**150-280**	**32 (8)**

In collision-dominated plasmas, both o- and x-mode EM waves suffer absorption given by the imaginary part of the complex refractive index *n*. The absorption per unit length κ is given by :

$$\kappa = \frac{f_p^2}{n} \frac{\nu_e}{(f \pm f_H \cos\theta)^2 + (\nu_e / 2\pi)^2} \qquad (2)$$

assuming that *n* is close to 1. The plus sign is for o-mode and the negative sign for x-mode, and θ is the angle between B_0 and the EM wave vector ***k***. This absorption, called non-deviative absorption, is most important in the D-region and lower E-region because, although the electron density N_e decreases by two to three orders of magnitude below the 100 km level, this is more than offset by the increase in ν so that the product in the numerator of (2) still increases by a factor of about 10. It results in heating of the plasma, i.e. of the electrons, by large amounts for powerful waves. Equation (2) shows that the absorption is a maximum in the vicinity of the altitude where

$$f \pm f_H \cos\theta = \nu_e / 2\pi \qquad (3)$$

Equation (2) implies that for most practically used frequencies (>3 MHz), the absorption decreases with increasing frequency. It is also clear that the absorption is large for an x-mode wave at the gyrofrequency (about 1.4 MHz).

Introduction to nonlinear effects

We can see from equation (2) that for heights above that where $\nu_e = \omega \pm \omega_H$, using angular frequencies and vertical incidence, the absorption, κ is $\sim \upsilon_e$ whereas below that κ is $\sim 1/\upsilon_e$. Since υ_e depends on T_e as:

$$\upsilon_e = \left\{1.7\times10^{-11}[\mathrm{N_2}]T_e + 3.8\times10^{-10}[\mathrm{O_2}]T_e^{1/2} + 1.4\times10^{-10}T_e^{1/2}\right\} \qquad (4)$$

(Dalgarno et al., 1967), which means approximately linear with T_e, a powerful EM wave modifies the medium in which it travels in a non-linear fashion. At some heights the medium becomes more opaque whereas at other heights more transparent, which requires a self-consistent calculation to determine the energy flux of a powerful wave at a given height.

Changing the electron temperature also changes the rate of some chemical reactions. For example, the recombination rate of electrons with molecular ions, α, is given by (Gurevich, 1978):

$$\alpha(T_e) = \frac{1}{N}\left\{5\times10^{-7}\left(\frac{300}{T_e}\right)^{1.2}[\mathrm{NO^+}] + 2.2\times10^{-7}\left(\frac{300}{T_e}\right)^{0.7}[\mathrm{O_2^+}]\right\} \qquad (5)$$

This shows that the electron density should increase as a result of a powerful HF wave, at least where molecular ions dominate.

Non-linear effects in collisional plasmas

Because the absorption coefficient depends on ν_e which depends approximately linearly with T_e, a powerful EM wave modifies the medium in which it travels in a non-linear fashion. At some heights the medium becomes more opaque whereas at other heights more transparent, which requires a self-consistent calculation. Basically one calculates T_e from the electron energy balance equation:

$$\frac{\partial T_e}{\partial t} = \frac{2}{3kN}(Q - L) \qquad (6)$$

where k is the Boltzmann constant, Q is the electron energy absorption rate due to HF heating, and L is the electron energy loss due to collisions. The Ohmic absorption rate, Q, is given by

$$Q = 2\kappa S N_e \qquad (7)$$

where S, the HF energy flux, is given by:

$$S(z) = \frac{ERP}{4\pi z^2}\exp\left\{-2\int_0^z \kappa(z')dz'\right\} \qquad (8)$$

Such calculations of the D-region absorption and electron heating are shown in the figure for several HF frequencies for both modes.

Note that the temperature changes are large compared to the ambient temperature which is of the order of 200 K. Although all this energy is eventually transferred to the ions and neutral molecules, the neutral temperature barely increases because the neutral density is about 11 orders of magnitude greater and the mass of the molecules is so much greater than the electron mass. The time constant involved depends on the neutral number density and T_e, but ranges from 10 μs at 60 km to 5 ms at 100 km.

HF-induced Te change and time constant in the lower ionosphere

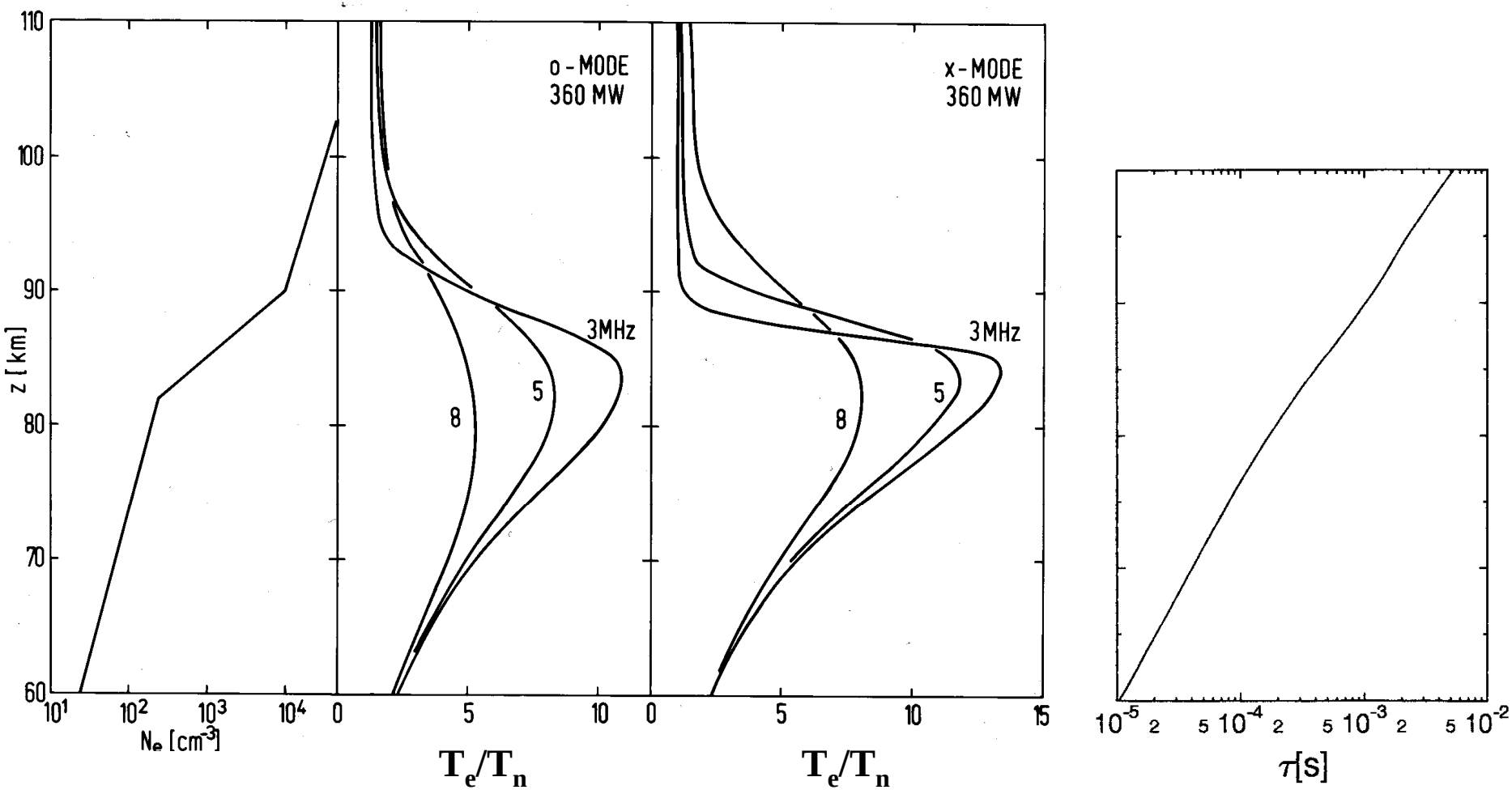

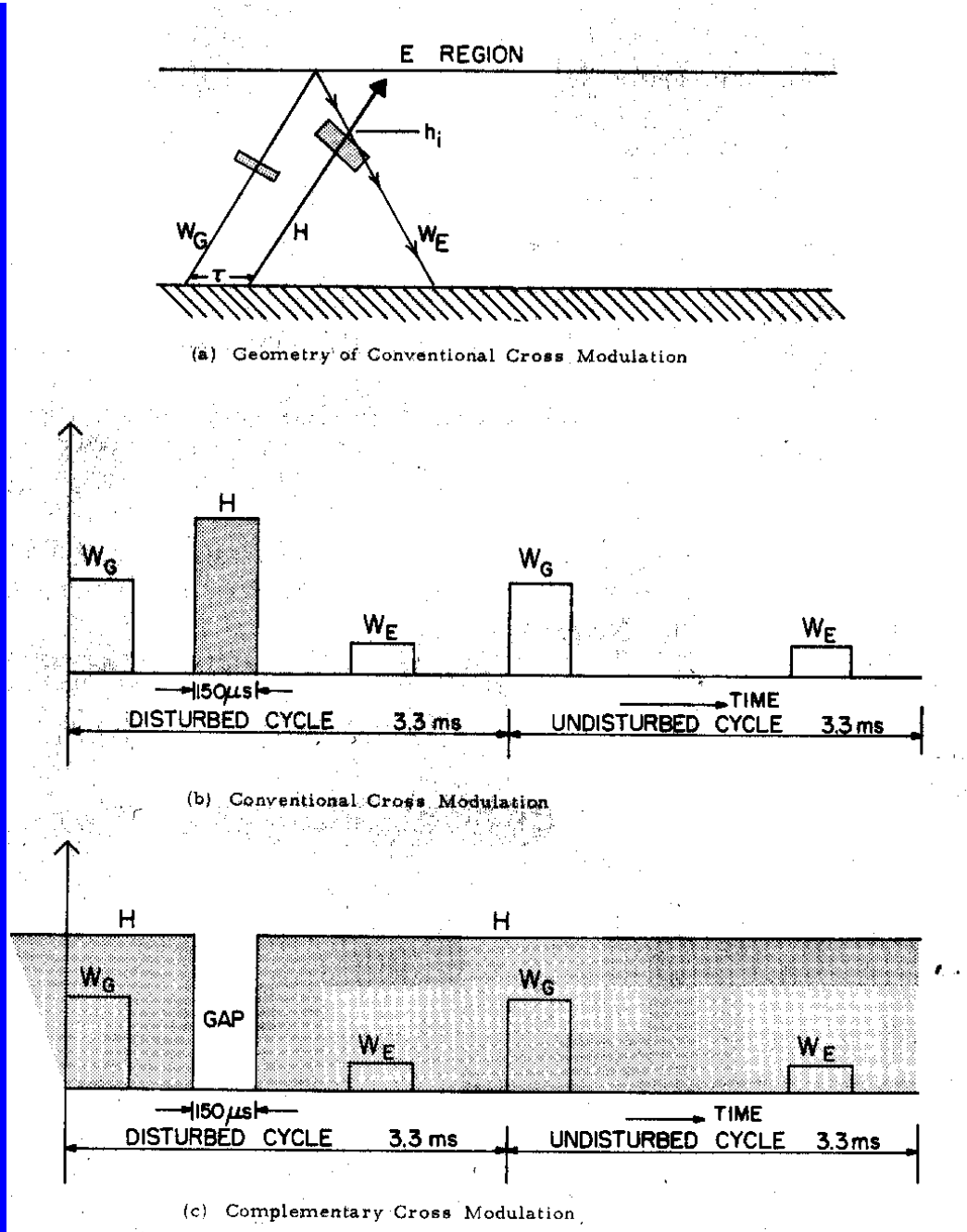

Fig. 1. Geometry and pulse sequence for conventional and complementary modes of cross modulation.

Complementary cross-modulation as a ”new” technique for studying ionospheric modification of the D region.

From Sulzer et al., JGR, 1976

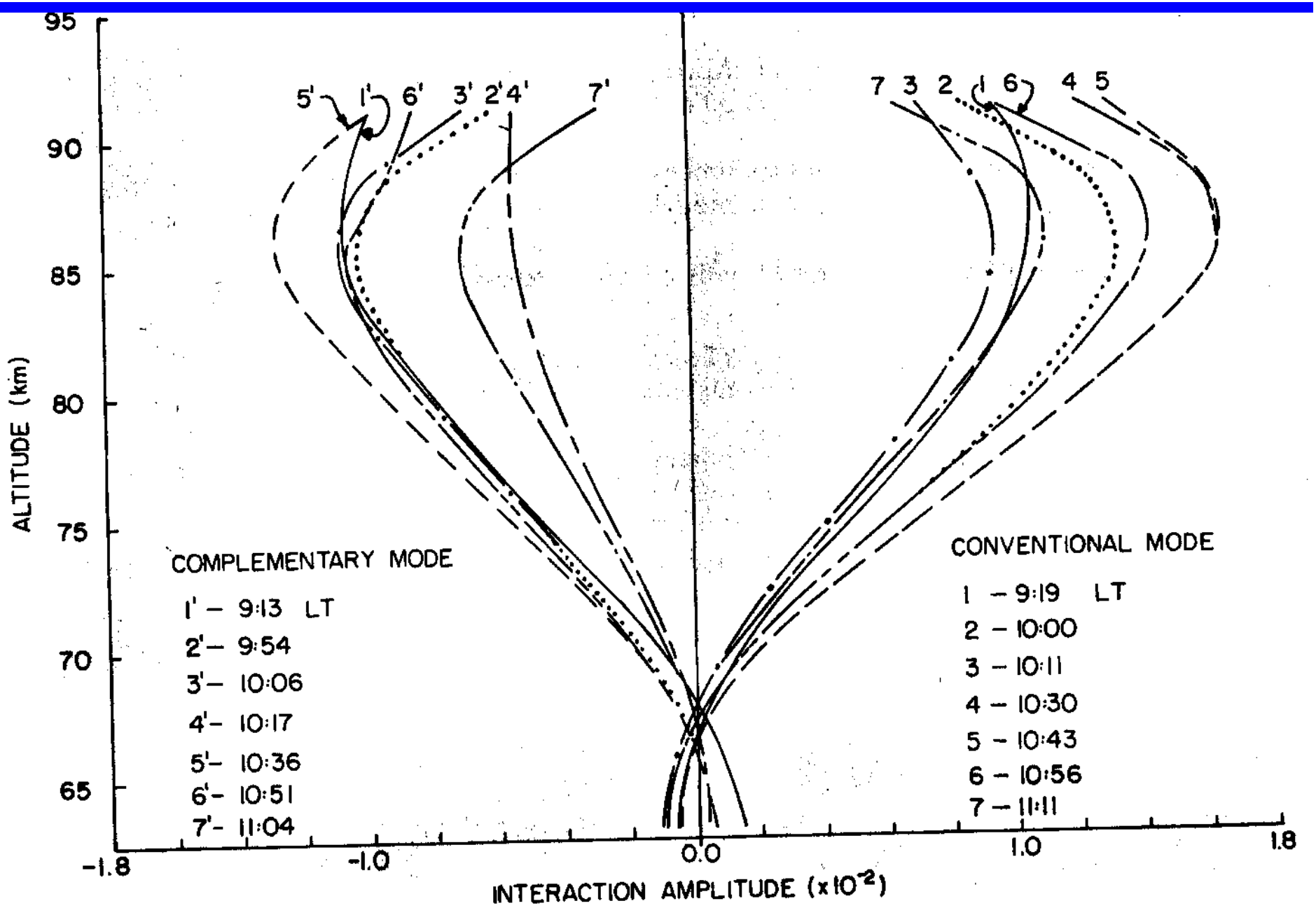

Fig. 2. Observed amplitude cross modulation for conventional and complementary modes.

Polar Mesospheric Summer Echoes (PMSE)

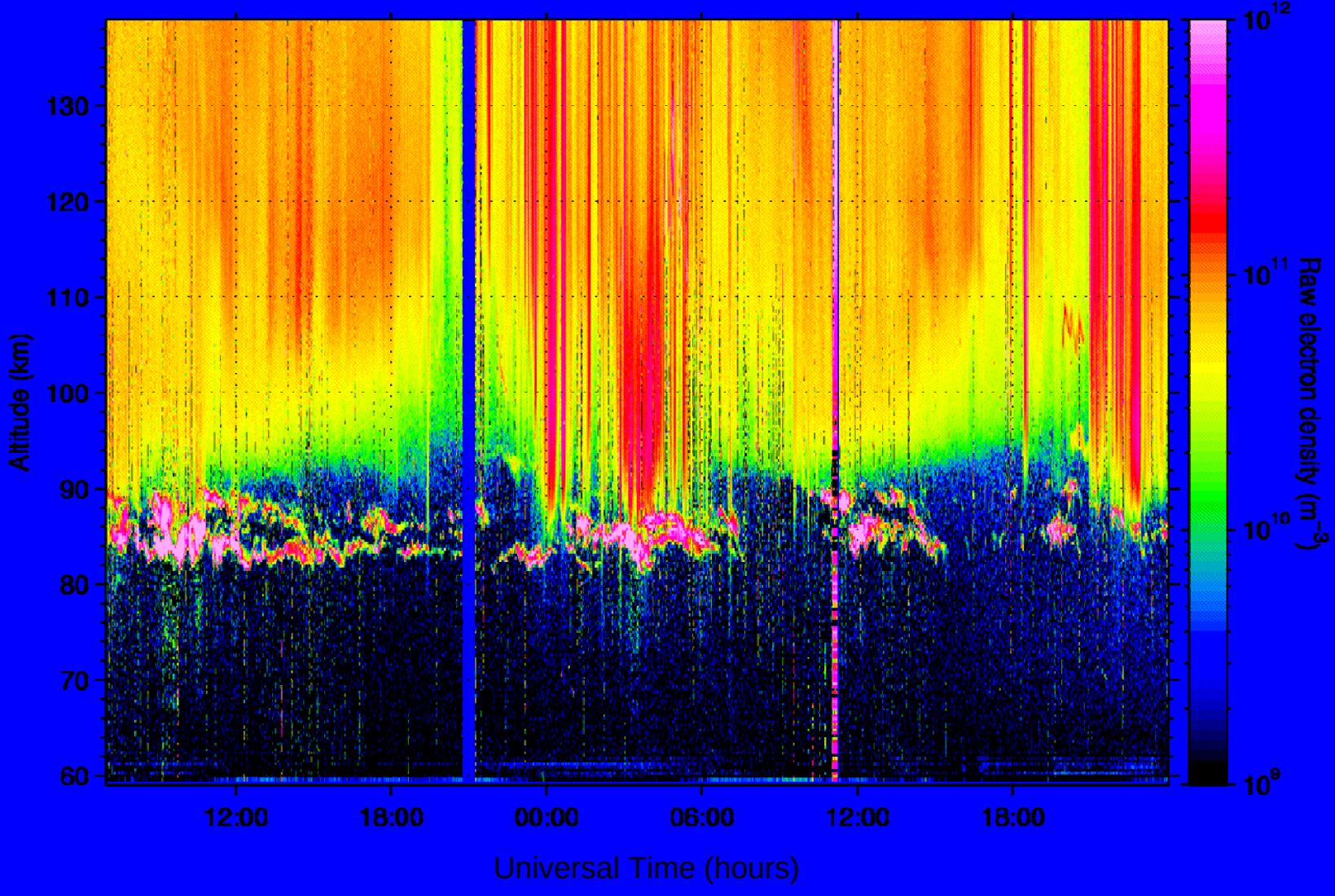

Relative location of NLC and PMSE

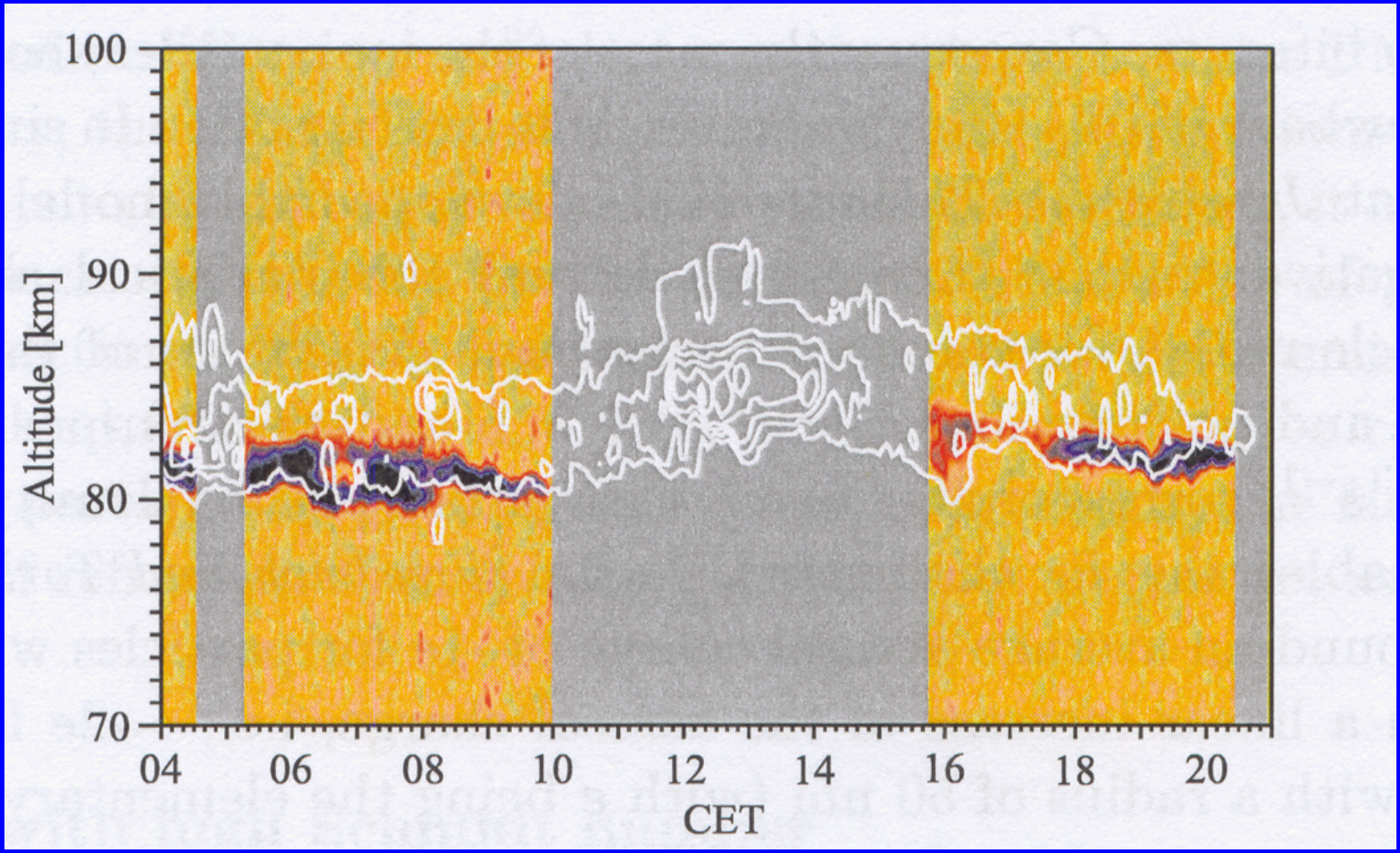

How does HF affect PMSE ?

PMSE weakening

•HF wave heats the electrons from about 150K to a few hundred K

•Heated electrons means density fluctuations smoothed out (increased diffusion). So PMSE weakens with HF on, and returns immediately with HF off.

PMSE Overshoot

•Dust (> 1nm particles) have electrons attached. The dust charging and electron gradients depend on particle size and density, electron density and electron temperature. The time time constant to discharge to undisturbed state during off is long.

•Useful diagnostic of dusty plasma since small particles charge slowly and large particles charge quickly.

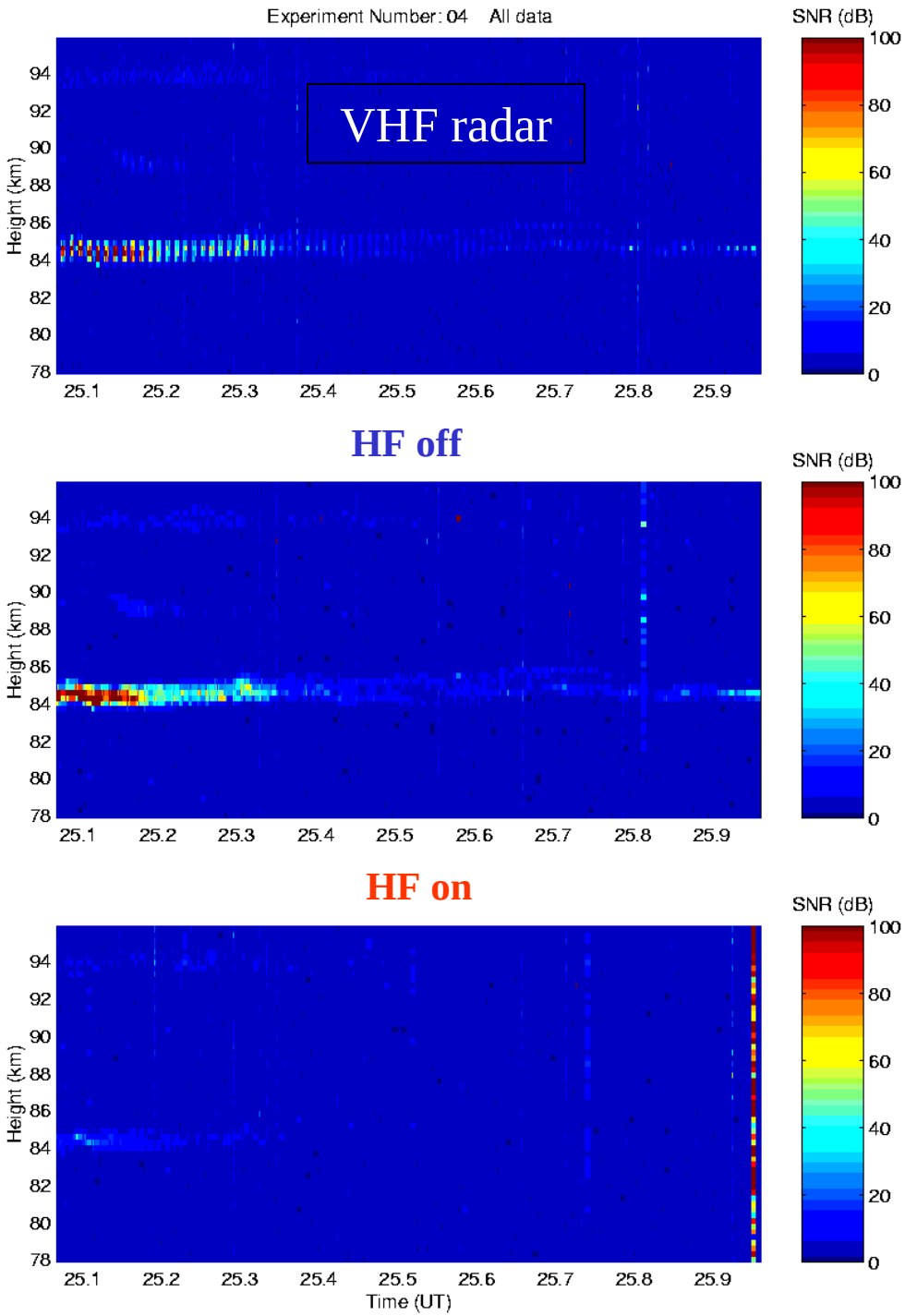

PMSE

Artificial HF modulation of Polar Mesospheric Summer Echoes. VHF backscatter power reduces by >40 dB. Reduction occurs on timescales less than 30 ms.

10 July 1999

5.423 MHz
ERP = 630 MW
X-mode
HF 10s ON, 10s OFF

Interpretation (see Rapp and Lübken, *GRL*, 2000)

•Increasing electron temperature compensates the effect of negatively charged aerosols on the diffusion of electrons. Increasing Te enhances electron diffusion and destroys PMSE. In terms of the Schmidt number, Sc, which is the ratio of kinematic viscosity to the effective diffusion coefficient of the electrons, $Sc = \nu/D_e^{eff}$ is reduced. Without aerosols $Sc \approx 1$.

•This is the **first direct experimental proof** that it is indeed the reduction of electron diffusion by charged aerosols which allows for the existence of scattering structures in the electron gas at very small scales.

•Using the particle charging model of Rapp and Lübken [2000] we find that an electron temperature increase also leads to an enhanced charging of the aerosols. Some of the aerosol particles acquire a second or even a third electron while for "normal" electron temperatures they are singly negatively charged. This implies that the total number of charges on the aerosol increases with increasing electron temperature. Increasing the aerosol charge, however, should support PMSE [Cho et al., 1992] al. Therefore this effect is minor.

•This experimental result does **not** help solve the real problem of PMSE, namely how can structures with these sizes exist in the aerosol gas.

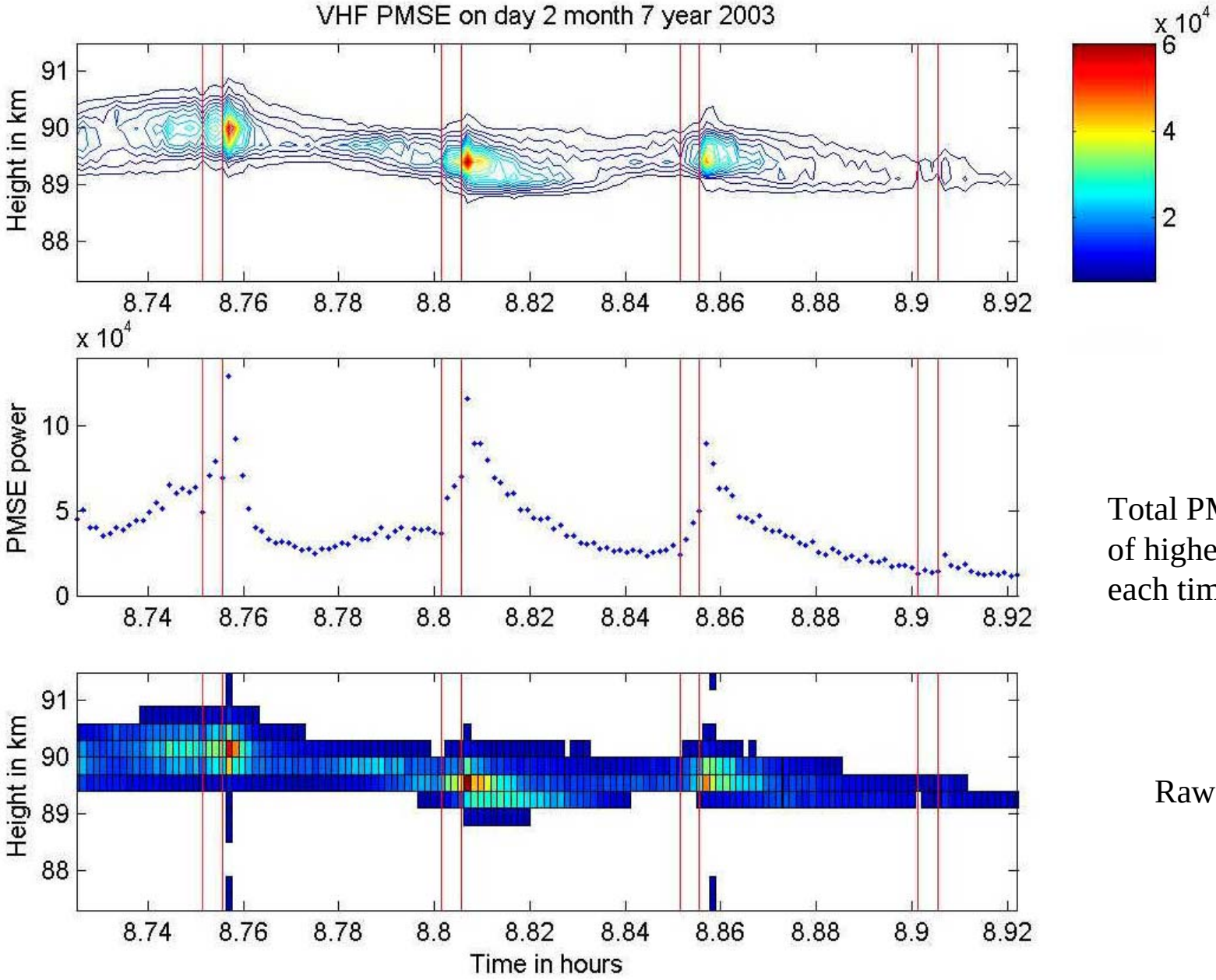

Smoothed data

Total PMSE intensity (sum of highest intensities at each time sample)

Raw data

PMSE echo strength showing an overshoot immediately after switch the 3s long heater pulse off. The background noise on this linear scale is at approximately 2500. (from Havnes et al., GRL, 30 2229, 2003.)

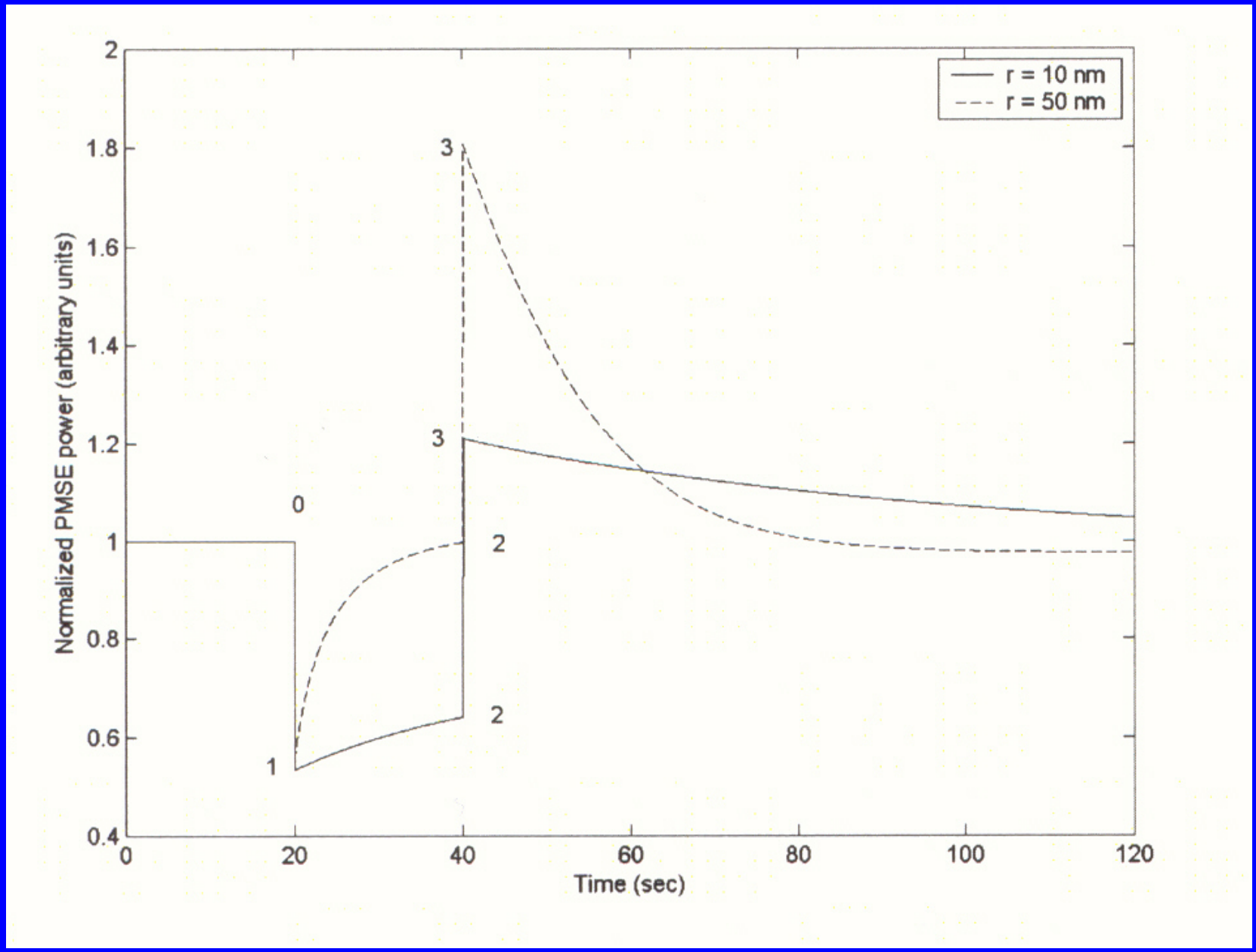

Model calculations showing how the shape of the overshoot phenomenon depends on particle size. HF is on from 20 to 40 s. The amplitude from 0 to 1 depends on the electron heating. (From Havnes et al., GRL, 2003)

PMWE

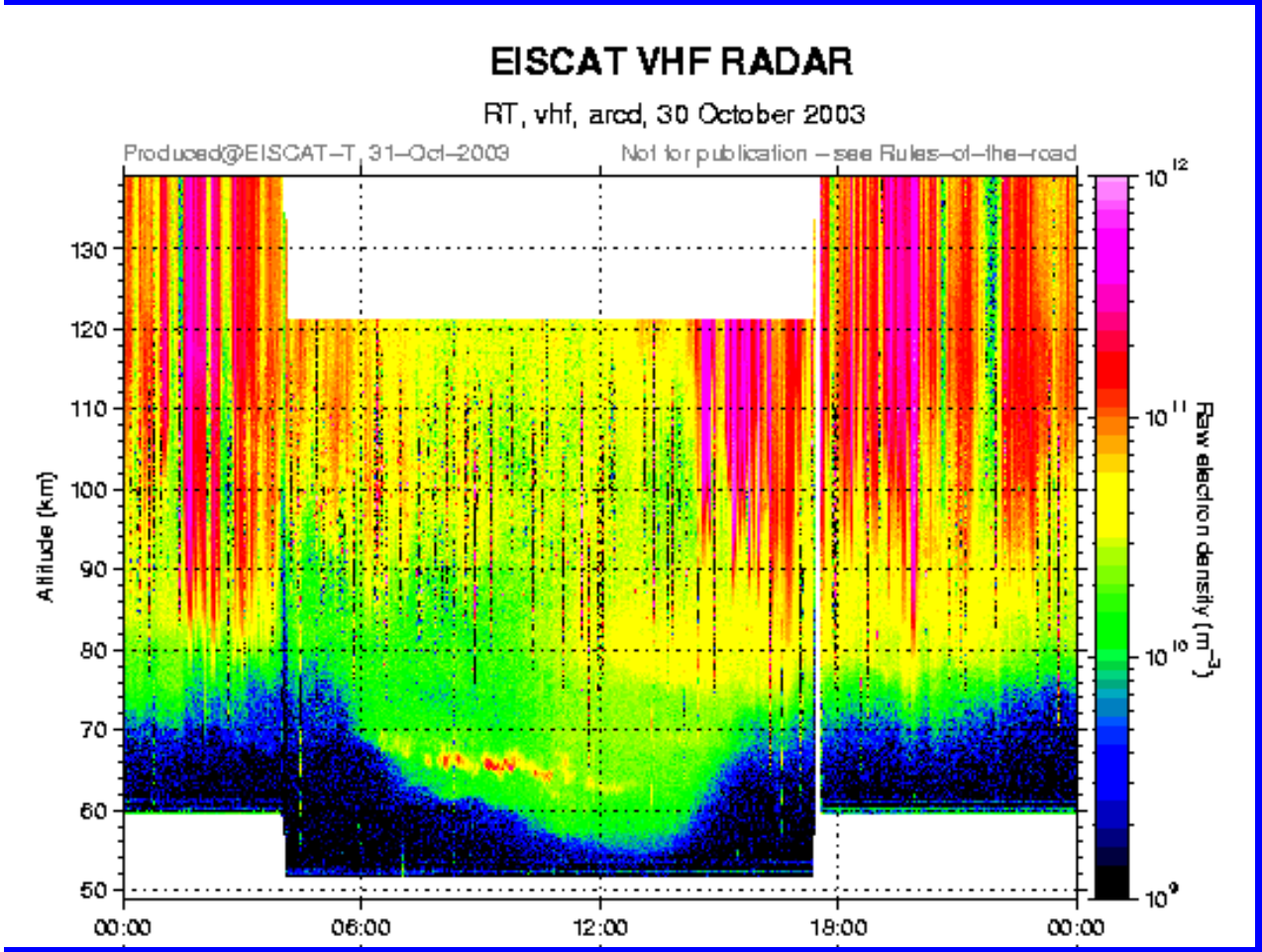

- Weaker than PMSE
- Lower altitude than PMSE
- Not followed by NLC
- Not during extreme cooling

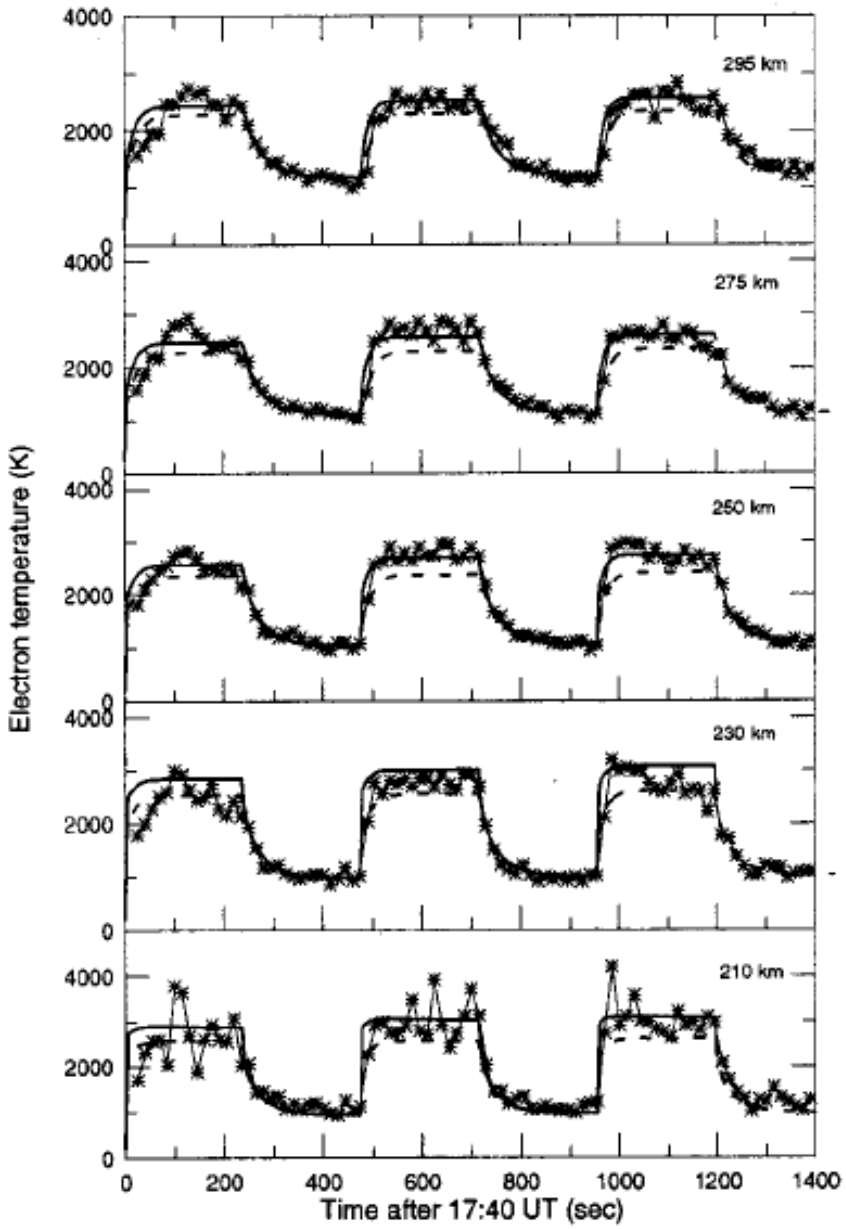

Fig. 3. Time variation of electron temperature at fixed altitudes. Asterisks give the EISCAT UHF radar measurements. Solid and dashed lines are modeled temperatures calculated for the different values of the electron heating source

HF-induced Te as a function of altitude.

From Sergienko et al., Phys. Chem. Earth, 2000.

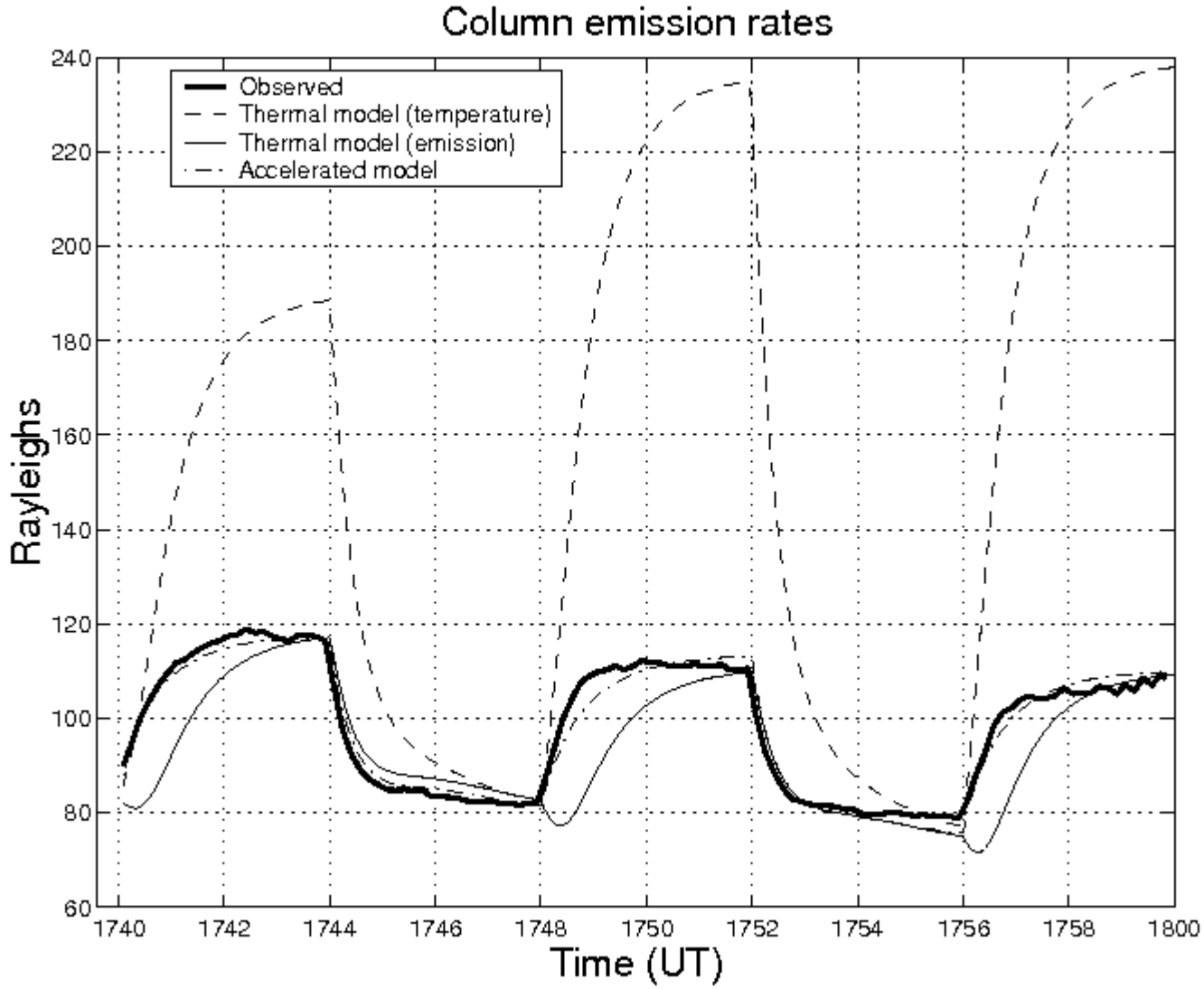
Column emission rates
Observed
Thermal model (temperature)
Thermal model (emission)
Accelerated model
Rayleighs
240
220
200
180
160
140
120
100
80
60
1740
1742
1744
1746
1748
1750
1752
1754
1756
1758
1800
Time (UT)

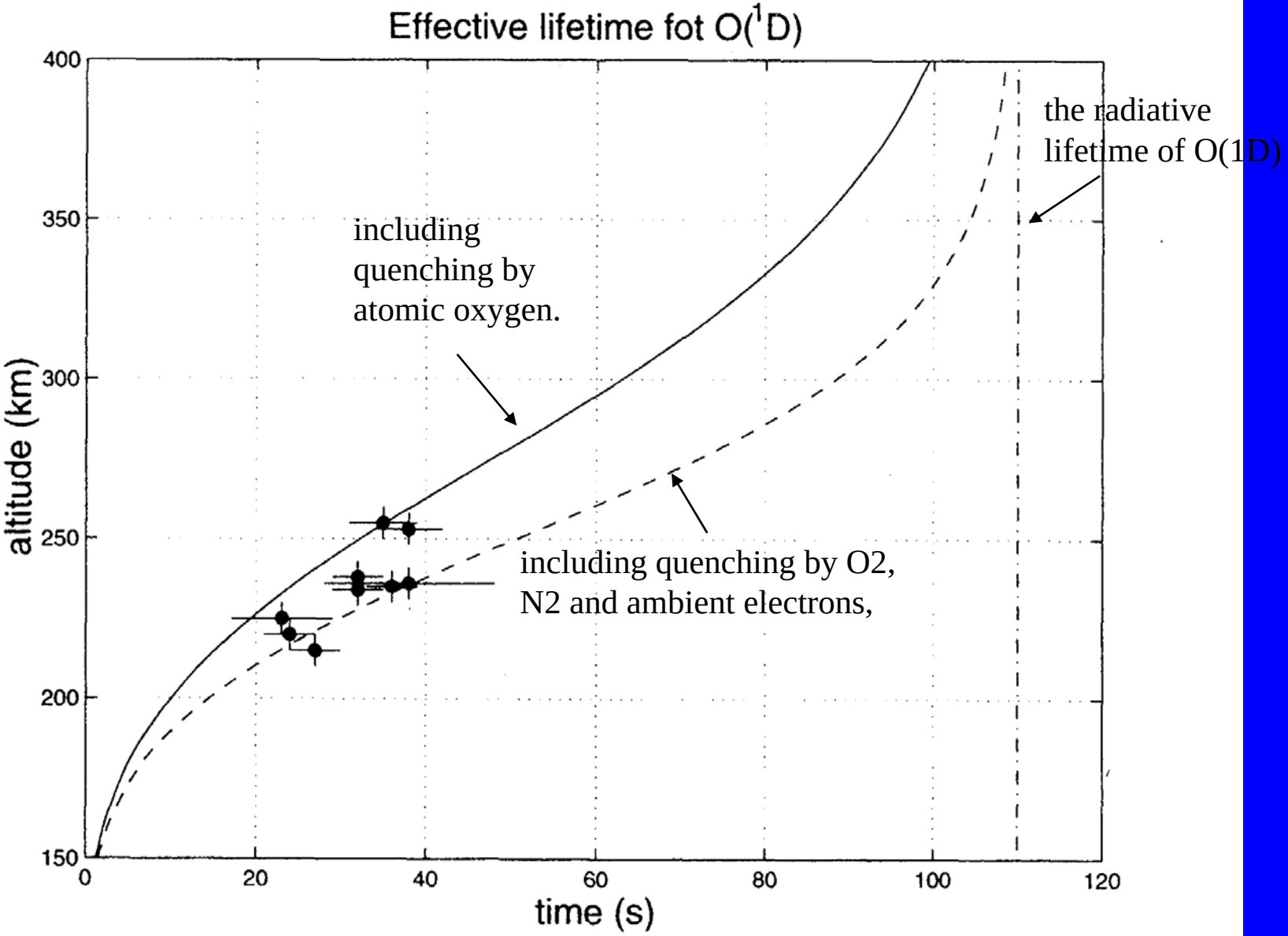

Altitude variation of the decay time constants of O(1D) from Bernhardt et al., JGR, 2000. The markers show estimates of the time constant from the experimental data. (from Gustavsson et al., J. Geophys. Res. 106, 29105-29124. 2001)

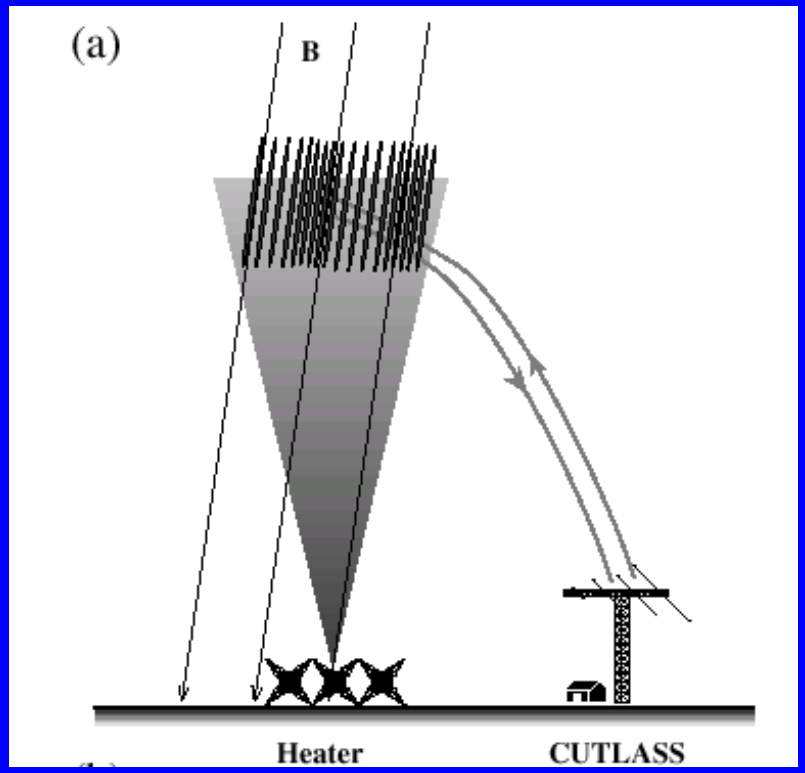

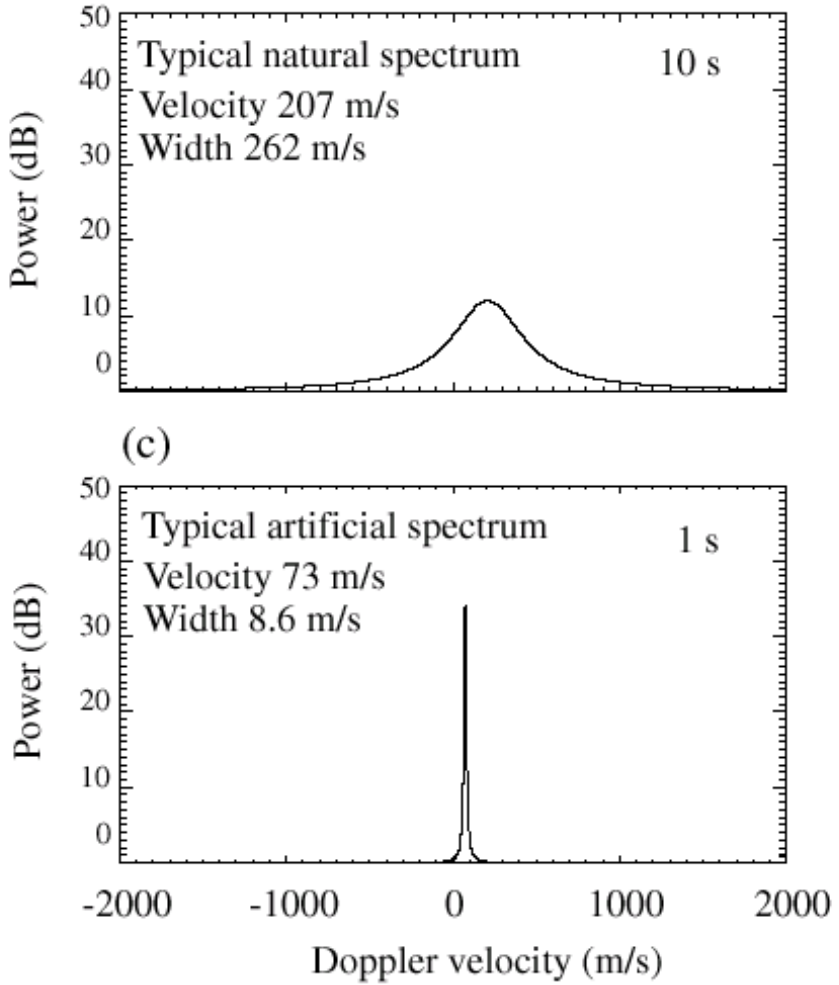

Fig. 1. **(a)** A schematic of the artificial backscatter experiment, SP-UK-OUCH. The Tromsø heater continuously heats the F region ionosphere, creating artificial ionospheric irregularities. These are detected by the CUTLASS radars, operating in a high temporal and spatial resolution mode. **(b)** A typical HF radar spectrum, obtained from fitting to the autocorrelation function of backscatter from natural F region irregularities after an integration period of 10 s. **(c)** A similar spectrum, but this time obtained from a 1 s integration from a heated F region. A narrower spectrum results, even from a shorter integration time.

From Yeoman and Wright, *Ann. Geophys.*, 2001

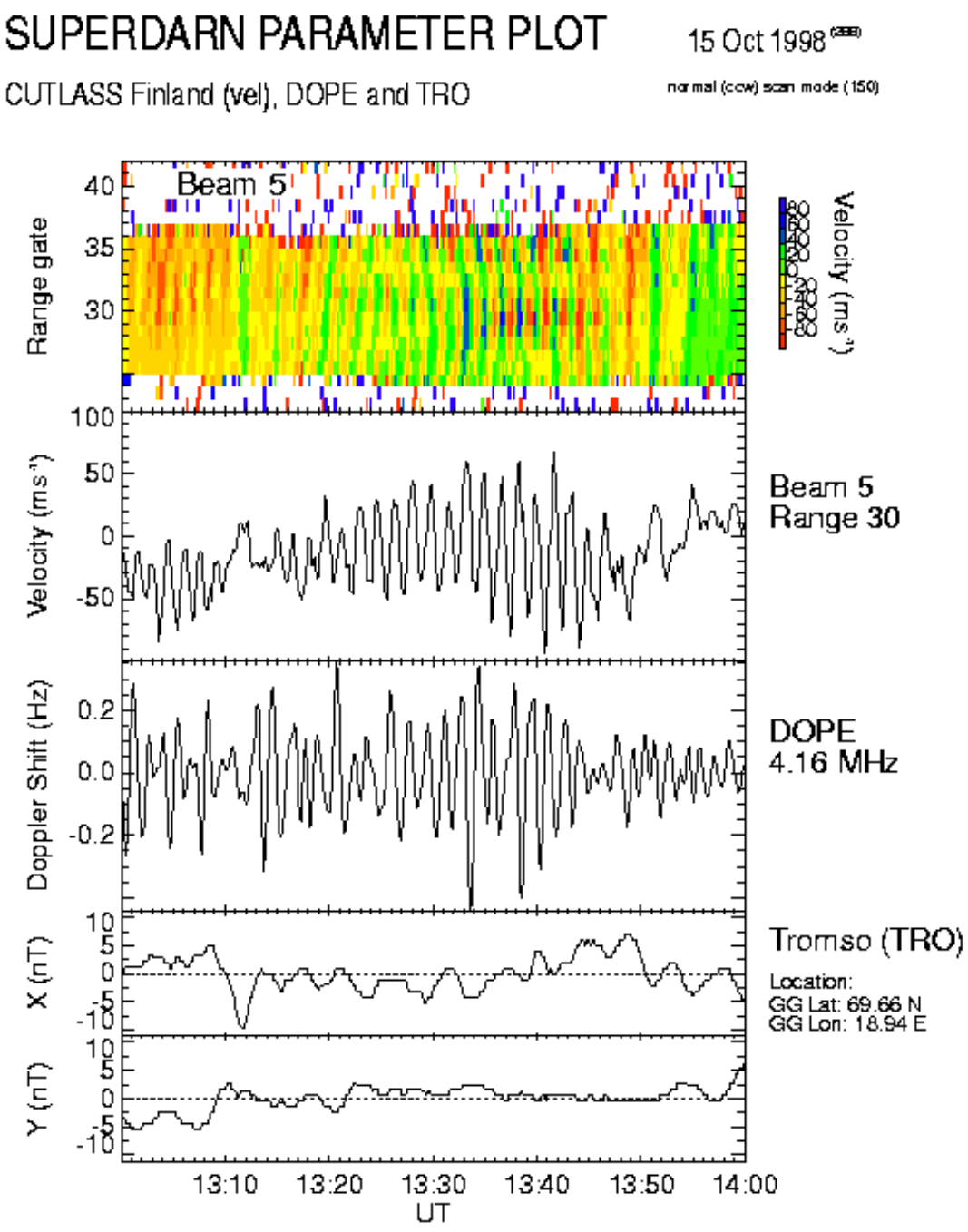

From Wright and Yeoman, *Ann. Geophys.*, 1999.

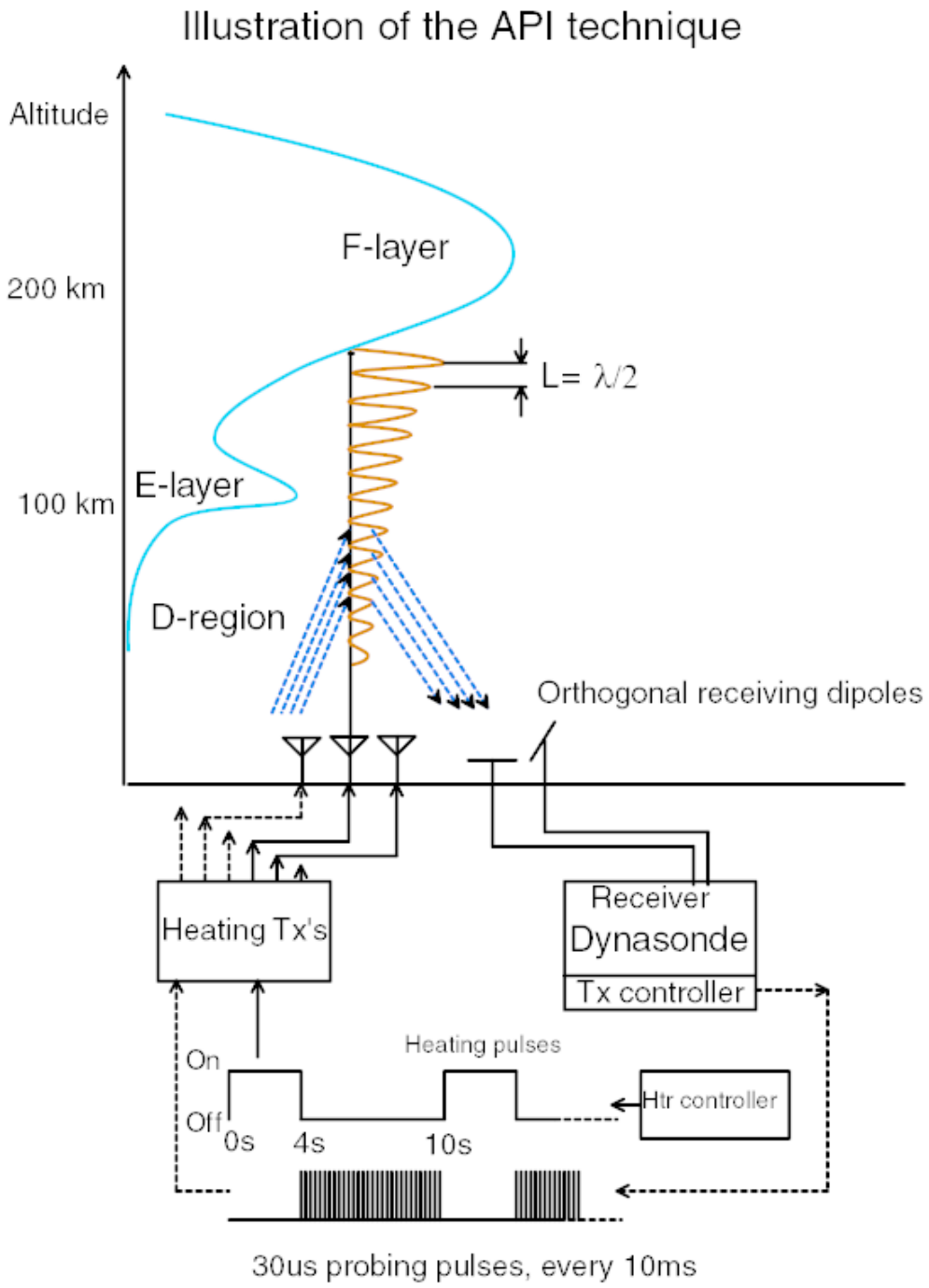

Artificial Periodic Irregularities (API)

The API technique was discovered at SURA and allows any HF pump and ionosonde to probe the ionosphere. API are formed by a standing wave due to interference between the upward radiated wave and its own reflection from the ionosphere.

(See book by Belikovich et al., 2001)

Measured parameters include: N(n), N(e), N(O-), vertical V(i), T(n), T(i) & T(e)

The Artificial Periodic Inhomogeneities (API) technique to study the mesosphere and the lower thermosphere

•API is a ground based technique for remote sounding of the ionosphere and atmosphere, discovered during HF-heating experiments in Russia in the 1970s.

•The API are formed by a standing wave that occurs due to interference between the upwardly radiated radio wave and its reflection off the ionosphere.

•The resonance Bragg backscatter from the API is observed from the heights where the disturbing and probing wavelengths are equal.

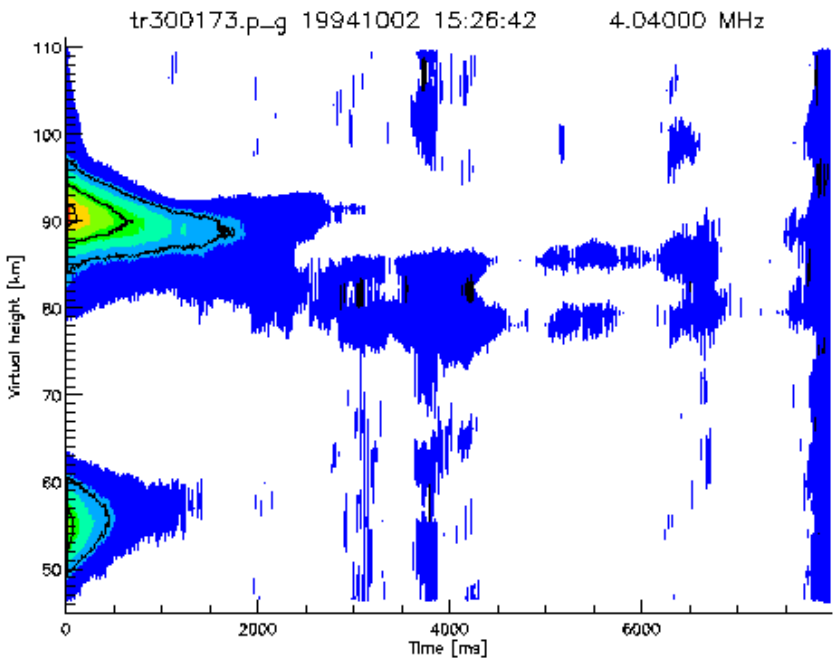

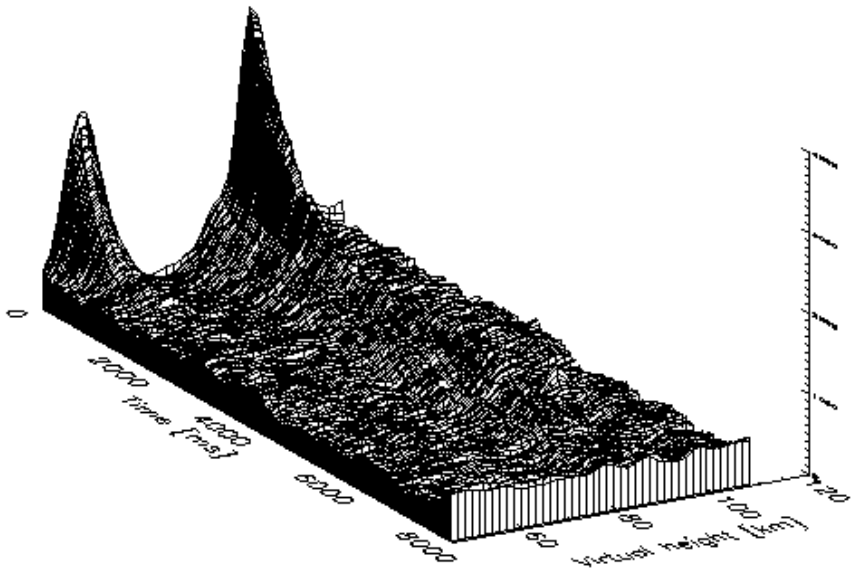

An example of API decaying in two altitude ranges, one rarely observed as low as 45-65 km, the other frequently observed between 80-100 km.

API Formation Mechanisms

- In the ionospheric F region API formation is due to ponderomotive force ($\propto E^2$) of the HF wave. Ion acoustic waves are excited which can be used to measure Ti and Te.
- In upper D and lower E region API are formed by the ambipolar diffusion of the ionospheric plasma differentially heated by the standing wave. Use this to determine neutral density and temperature.
- Atmospheric turbulence has an effect on the processes of the API formation and decay, so that the turbopause height, where the transition from molecular to eddy diffusion takes place, can be found.
- In the lower D region (below approximately 75 km) negative ion chemistry reactions are modulated by the heated electrons.

Information derivable from the API technique

- profiles of the electron density from the lower D-region up to the F-layer maximum
- vertical velocities in the D- and E-regions of the ionosphere
- irregular structure of the ionosphere including the separation of the regular E-layer, the sporadic layers, additional layers in the valley
- parameters of turbulence: the turbulent velocities, the turbulent diffusion coefficients and the turbopause height
- to study sunset-sunrise transition
- neutral temperatures and densities at E-region heights
- relative concentration of negative oxygen ions in the D-region
- effect and parameters of internal gravity waves and their spectral characteristics
- electron and ion temperatures, T_e,T_i, in the F-region

Conclusions

There is much potential in exploring D-region chemistry by means of:

- Wave-Interaction technique
- Incoherent scatter
- Heating effects on PMSE/PMWE echoes.
- API technique
- ELF/VLF wave generation

- HF-induced irregularities are a sensitive tracer of ULF electric fields
- F region aeronomy models can be tested using HF-induced electron temperature and artificial optical emission time constants.